Response to Review 2

We thank the reviewer for the detailed comments which helped to improve the manuscript. Most of the suggestions were gratefully taken up. Please note that numbering for figures and tables is changed because now the Appendix is moved into section 2.2 (Methodology of Method 2) by following the reviewer's suggestion. In addition, calibration results are now presented for each month following both reviewers' comment. We changed the way to compare three methods in the revised version; i.e. we compared regression results instead of mean biases. This is because many targets used for Method 1 have near-zero reflectances, which cause large uncertainties in estimating relative differences between measured and reference reflectances.

However, most of main conclusions of this paper were not changed. One exception is that we now see Meteosat-8 comparable to Meteosat-9 on a monthly basis.

General comments

The authors describe three methods to assess the calibration accuracy of the visible channel of MET-8/9 centred at 646nm and of MTSAT-1R centred at 724nm and present an application to some months of data. The methods exploit 1) collocations between these two geostationary satellite sensors and the polar-orbiting MODIS instrument; 2) radiative transfer simulations of satellite reflectances starting from MODIS cloud properties; 3) deep convective cloud targets. As a result, relative accuracies are found to lie within 5–10% for MET-8, 4–9% for MET-9 and up to 20% for MTSAT-1R.

This interesting paper addresses an important topic not only for climate research but also for process studies related to cloud physical properties. Although it is well written, important changes must be carried out. Thus, this paper should be published in ACP but it must first go through major revisions (see below).

Specific comments

The main deficiencies of the paper consist in

1. the illustration of the methods

2. the application of the methods

3. the missing evaluation of the results against literature results.

In the following, I will go through these points.

Method 1

1. The theoretical relationships between the two sensors' reflectances that are used to take

into account differences in spectral response functions are a very important tool to correctly evaluate calibration uncertainties. However, their derivation is only roughly sketched and necessary details about these radiative transfer calculations are missing and should therefore be added to the manuscript. First of all, not only the range of the sun-satellite geometry should be given but also the way how this range is sampled (How many sample points have been used? Are these sample points equally separated or random distributed?). Since only ocean pixels were collocated, I imagine that an ocean surface was assumed for the simulations. Is this really so? Which parameterization was used for the ocean BRDF? If the BRDF depends on wind for the consideration of white caps, which wind speed was used? The cloud phase was also not mentioned: are you considering only water clouds or also ice clouds? In case: Why did you select only water clouds? How did you parameterised optical properties of ice crystals? While you talk about a RTM, you do not mention which RTM you used. Is it SBDART? Furthermore, gas absorption must be correctly accounted for, usually by means of a correlated-k method. Which one did you use? How many sample points were considered for the single satellite channels? Since ozone absorption and water vapour absorption affect measurements in the given spectral intervals it is also important to mention which atmospheric profiles were used. Although not essential, the indication of the vertical cloud location inside the atmosphere (cloud bottom and cloud top heights) are also desirable. Finally, the overall number of radiative transfer calculations performed should be mentioned. Please clarify these issues.

Following the suggestions, detailed description of radiative transfer modeling is now provided.

[Old]

Because the SRF determines the magnitude of gas absorption and scattering, cloud extinction, and surface reflectance for the given SRF band, the spectral differences between SRFs should be considered for the inter-comparison. Theoretical relations between two sensors were obtained from radiative transfer simulations. For the simulation, various conditions with changes of the SZA (from 0 to 40°), VZA (from 0 to 40°), relative azimuth angle (from 0 to 180°), effective radius (10, 20, and 30 μm), and cloud optical thickness (COT) (0, 5, 10, 20, 40, 60, 80, and 100) were used as inputs for the RTM.

[New]

Because the SRF determines the magnitude of gas absorption and scattering, cloud extinction, and surface reflectance for the given band, the spectral differences between SRFs should be considered for the inter-comparison. To obtain theoretical relations between two sensors, radiative transfer simulations are performed using Santa Barbara Disort Radiative Transfer (SBDART; Ricchiazzi et al., 1998) model. In the simulation, surface type is

assumed to be ocean since calibration targets are collected only over ocean. Then oceanic bidirectional distribution function (BRDF) model is used for obtaining surface reflectance with 0.1 mg m^{-3} of pigment concentration, 5 m s^{-1} of wind speed, and 34.3‰ of salinity. Note that the oceanic BRDF model provided in SBDART is nearly same as the one used in Second Simulation of Satellite Signal in the Solar Spectrum (6S) RTM (Vermote et al., 1997). One difference is that the BRDF in SBDART is independent of wind direction because of the average of 6S BRDFs for all azimuth angles (Ricchiazzi, 2002). For estimating the gas absorption for each channel, LOWTRAN 7-based transmittances (Pierluissi and Peng, 1985) are used with three-term exponential fitting (Ricchiazzi et al., 1998). Temperature, pressure, water vapor, and ozone profiles are described from standard tropical profiles, with an assumption that all collocated targets are located between 20°N and 20°S, satisfying SZA ≤ 40° and VZA ≤ 40°.

For cloudy sky, scattering properties of water droplets are obtained from Mie calculations, while scattering properties of ice habits are described from Baum et al. (2005a, 2005b; hereafter Baum scattering model). Baum scattering model provides bulk scattering properties of nonspherical ice particles, based on field experiments (Heymsfield et al., 2002) and theoretical scattering computations (Yang et al., 2003, 2005). The Baum and Mie scattering models provide scattering parameters such as extinction efficiency, single scattering albedo, asymmetry factor, and phase function with respect to particle effective radius for the given spectral channel. Because the phase function associated with large cloud particles has a strong forward peak, thousands of Legendre terms are required to take into account full scattering phase function in the simulation (King, 1983; Nakajima and Tanaka, 1988; Hu et al., 2000). Therefore, delta-transmission and diffraction peaks of the phase function are truncated (Wiscombe, 1977; Yang et al., 2000) for accurate and efficient calculation with 20 streams in RTM.

With provided scattering parameters, three particle effective sizes of 10, 20, and 30 μm are considered in the simulation. Moreover, 8 cases of cloud optical thickness (COT) (0, 5, 10, 20, 40, 60, 80, and 100) are used, including clear sky case (COT = 0), while cloud altitude is assumed to reside between 11 km and 12 km. Also various solar and viewing geometries are considered with changes of the SZA (=0, 10, 20, 30, and 40°), VZA (=0, 10, 20, 30, and 40°), relative azimuth angle (RAA) (=0, 10, 20,…, 170, and 180°). Finally, total 22,800 combinations (i.e. 2 cloud phases × 3 effective sizes × 8 COTs × 5 SZAs × 5 VZAs × 19 RAAs) are considered for the single channel calculation.

Figure 2 shows spectral relations between two channel reflectances from simulation results. Strong linear relationships are shown regardless of input conditions, suggesting that the regression equation can be reliably used to convert MODIS channel reflectances into reflectances for channels of different sensors.

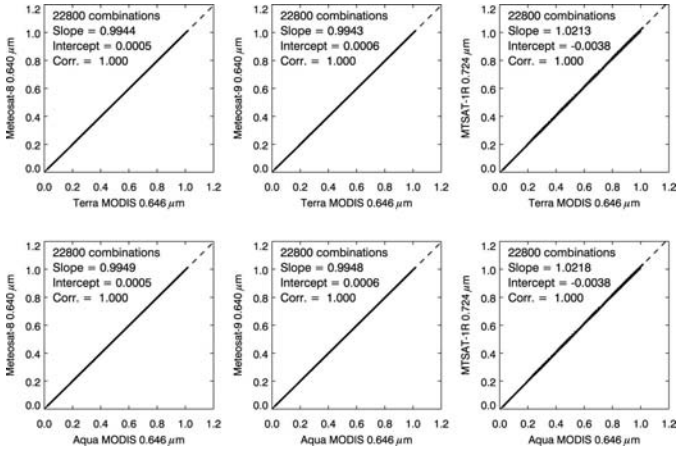

Fig. 2. Spectral relations between two channels. (top) Meteosat-8 and Meteosat-9 0.640-μm, and MTSAT-1R 0.724-μm channels relating to Terra MODIS 0.646-μm channel. (bottom) Meteosat-8 and Meteosat-9 0.640-μm, and MTSAT-1R 0.724-μm channels relating to Aqua MODIS 0.646-μm channel.

Hu, Y. X., Wielicki, B., Lin, B., Gibson, G., Tsay, S.-C., Stamnes, K., and Wong, T.: δ-Fit: A fast and accurate treatment of particle scattering phase functions with weighted singular-value decomposition least-squares fitting, *J. Quant. Spectrosc. Radiat. Trasfer,* **65,** 681–690, 2000.

King, M. D.: Number of terms required in the fourier expansion of the reflection function for optically thick atmospheres. *J. Quant. Spectrosc. Radiat. Trasfer*, **30,** 143–161, 1983.

Nakajima, T., and Tanaka, M.: Algorithm for radiative intensity calculations in moderate thick atmospheres using a truncation approximation, *J. Quant. Spectrosc. Radiat. Trasfer*, **40,** 51–69, 1988.

Ricchiazzi, P., Yang, S., Gautier, C., and Sowle, D.: SBDART: A research and teaching software tool for plane-parallel radiative transfer in the Earth's atmosphere, *B. Am. Meteor. Soc.*, **79,** 2101–2114, 1998.

Ricchiazzi, P.: Input documentation for SBDART, Univ. of California, Santa Barbra, 2002.

Vermote, E. F., Member, IEEE, Tanre, D., Deuze, J. L., Herman, M., and Morcrette, J.-J.: Second Simulation of the Satellite Signal in the Solar Spectrum, 6S: An overview, *IEEE T. Geosci. Remote Sens.*, 35, 675-686, 1997.

Pierluissi, J. H., and Peng, G.-S.: New molecular transmission band models for LOWTRAN, *Opt. Eng.,* **24** (3), 541–547, 1985.

Heymsfield, A. J., Bansemer, A., Field, P. R., Durden, S. L., Stith, J., Dye, J. E., Hall, W., and Grainger, T.: Observations and parameterizations of particle size distributions in deep tropical cirrus and stratiform precipitating clouds: Results from in situ observations in TRMM field campaigns, *J. Atmos. Sci.*, 59, 3457–3491, 2002.

Wiscombe, W. J.: The Delta-M Method: Rapid yet accurate radiative flux calculations for strongly asymmetric phase functions, *J. Atmos. Sci.,* **34,** 1408–1422, 1977.

Yang, P., Liou, K. N., Wyser, K., and Mitchell, D.: Parameterization of the scattering and absorption properties of individual ice crystals, *J. Geophys. Res*., **105,** 4699–4718, 2000.

Yang, P., Baum, B. A., Heymsfield, A. J., Hu, Y.-X., Huang, H.-L., Tsay, S.-C., and Ackerman, S. A.: Single scattering properties of droxtals, *J. Quant. Spectrosc. Radiat. Transfer*, **79-80**, 1159–1169, 2003.

Yang, P., Wei, H., Huang, H.-L., Baum, B. A., Hu, Y.-X., Kattawar, G. W., Mishchenko, M. I., and Fu, Q.: Scattering and absorption property database for nonspherical ice particles in the near- through far-infrared spectral region, *Appl. Opt.*, **44,** 5512–5523, 2005.

2. While MODIS is calibrated against reflectances (MODIS is a reflectometer) and these reflectances are directly available in the MOD02/MYD02 products, SEVIRI reflectances must be computed starting from radiances under the assumption of some solar constant value. Please specify the values used in this study.

Now solar constant values are provided for Meteosat-8 and Meteosat-9 0.640-μm channels.

[Old]

In this study, the 0.640-μm and 11-μm channels, provided at a 4.8-km spatial resolution, were used to examine the calibration status of the SEVIRI visible channel.

[New]

In this study, the 0.640-μm and 11-μm channels, provided at about 3-km spatial resolution, are used to examine the calibration status of the SEVIRI visible channel. Radiances at 0.640-μm channels are converted into reflectances using solar irradiances at the band, i.e. 1617.45 W m^{-2} μm^{-1} for Meteosat-8 and 1617.03 W m^{-2} μm^{-1} for Meteosat-9 (Govaerts et al., 2006) with the consideration of Sun-Earth distance and solar zenith angle (SZA).

Govaerts, Y., Wagner, S., Clerici, M.: SEVIRI native format pre-processing toolbox user's guide, Issue: SPT Version 2.4, No: EUM/OPS-MSG/TEN/03/0011, EUMETSAT, Germany, 2006.

3. An indication about the spatial (and temporal) distribution of the collocations as well as their number should be given.

Figure D1 represents spatial/temporal distribution of the calibration targets for Method 1. Due to restrictions of smaller SZA (≤ 40°) and VZA (≤ 40°), and imposed conditions for the

ray-matching, all targets are located near equator. For each month, more than 1000 targets are chosen and their locations near the equator change little from season to season. The number of chosen targets is now found in the scatter plots. Changes are following:

[Old]

The measurements of SEVIRI 0.640-μm channels aboard Meteosat-8 and Meteosat-9 were compared against the MODIS 0.646-μm channel by applying Method 1. MODIS-equivalent SEVIRI 0.640-μm channel reflectances were obtained by using Eqs. (1)−(4). Although four months of data were used for each satellite comparison, a relatively small number of targets were selected because of the limited number of cases that satisfied the imposed conditions for ray-matching.

[New]

The measurements of SEVIRI 0.640-μm channels aboard Meteosat-8 and Meteosat-9 are compared against the MODIS 0.646-μm channel by applying Method 1. MODIS-equivalent SEVIRI 0.640-μm channel reflectances are obtained by using Eqs. (1)−(4). Regardless of the season, all collocated targets are selected from the area of 40°W–40°E and 20°N–20°S, satisfying smaller SZA (≤ 40°), VZA (≤ 40°) and imposed conditions for the ray-matching.

In addition, spatial distribution of targets for the MTSAT-1R calibration is also discussed.

[New]

Throughout the seven-month period, all collocated targets for MTSAT-1R are located in the area of 100°E–180°E and 20°N–20°S.

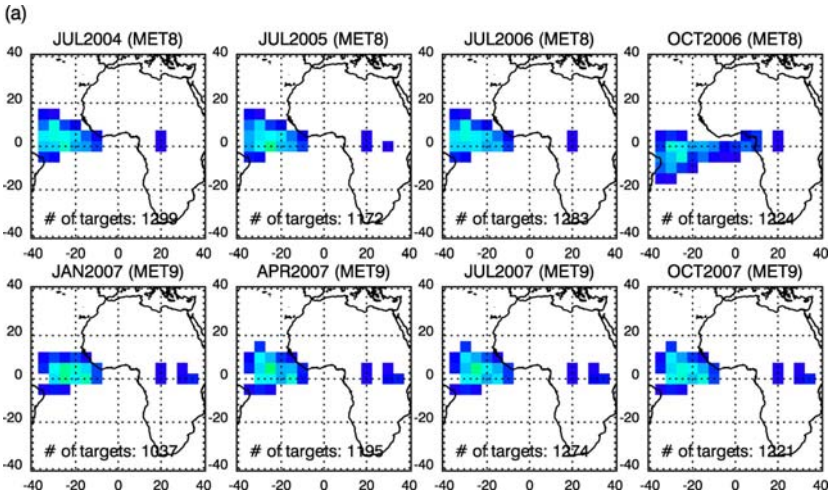

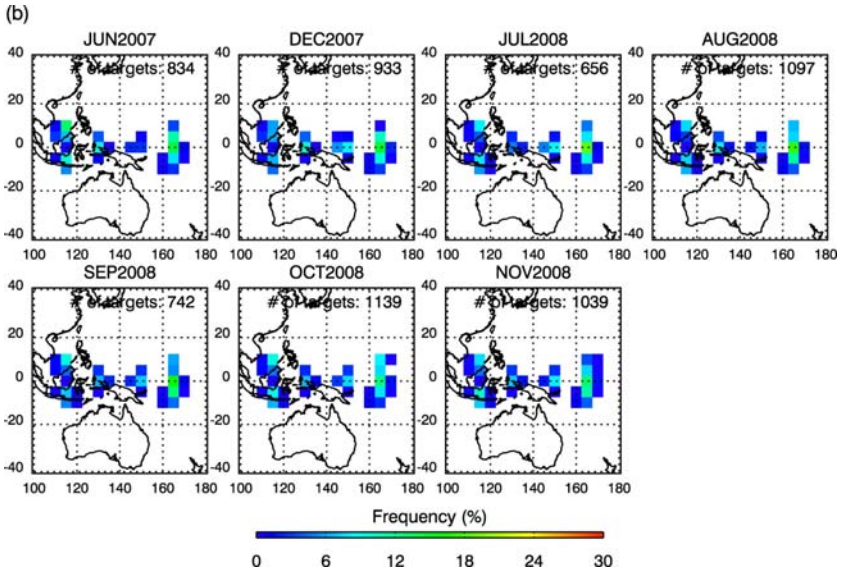

Figure D1. Spatial distribution of chosen calibration targets for Method 1 applied to (a) Meteosat-8/9 and (b) MTSAT-1R visible channels.

4. Furthermore, it should be explained why MODIS band 1 and not MODIS band 15 (743–753 nm) was selected for the calibration of the MTSAT-1R visible channel centred at 724 nm.

MODIS band 15 is designed for ocean color retrieval, and thus has a low saturation level, under 100 W m^{-2} μm^{-1} sr^{-1}. Thus the band 15 may not be adequate for testing the calibration status of other satellite using cloud targets, although the spectral location appears to be closer to the MTSAT-1R 0.724-μm channel, in comparison to the band 1.

5. Please provide a plot of all three (four) spectral response functions (MODIS, SEVIRI-8/9, MTSAT-1R).

SRFs of all five channels are provided in Fig. 1.

[New]

SRFs of MODIS, Meteosat-8/9, and MTSAT-1R visible channels are compared to each other in Fig. 1. MODIS 0.646-μm channels show a narrow spectral coverage between 0.6 μm and 0.7 μm, while MTSAT-1R 0.724-μm channel shows a broad spectral coverage from 0.55 μm to 0.9 μm. It seems that two MODIS channels aboard Terra and Aqua have negligible spectral differences, and so do two SEVIRI 0.640-μm channels aboard Meteosat-8 and Meteosat-9.

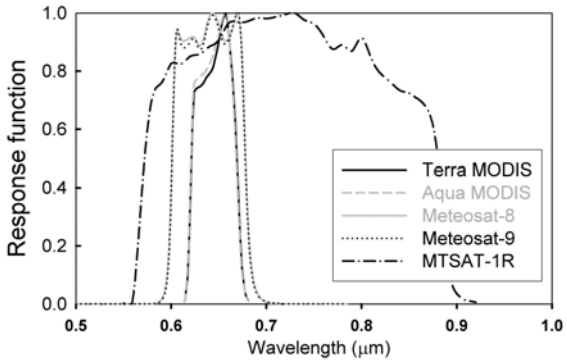

Fig. 1. SRFs of MODIS 0.646-μm channels aboard Terra and Aqua, SEVIRI 0.640-μm channels aboard Meteosat-8 and Meteosat-9, and MTSAT-1R 0.724-μm channel.

Method 2

6. The relatively simple use of CTT thresholds for the distinction between water and ice clouds seems not very reliable. In principle, a MODIS cloud top phase product is also available and represents the basis for the determination of cloud optical thickness of the MODIS algorithm. Thus, this quantity should have been used instead of or in addition to the CTT threshold tests mentioned in the manuscript. Please comment on this.

Now basis of CTT threshold values is explained.

[Old]

The cloud top temperature (CTT) at each grid was used to determine the cloud phase. For CTT ≥ 273 K, Mie scattering was used for the radiative simulation by assuming spherical water particles of the cloud. For CTT ≤ 227 K, scattering properties of Baum et al. (2005a, b) were considered for nonspherical ice particles of the cloud. The threshold value of 227 K for ice clouds was based on the fact that the MODIS cloud phase algorithm mostly detects ice cloud when CTT ≤ 227 K.

[New]

To determine the dominant cloud phase at a 0.5°-grid box, grid-averaged cloud top temperature (CTT) is used. The threshold conditions of CTT are prepared based on two-month (June and December 2007) MODIS data over 100°E–180°E, 40°N–40°S area. In Fig. 3, using MODIS cloud phase products (“Cloud_Phase_Infrared”) provided at a 5-km resolution, frequency distributions of CTT are separately obtained for ice and water clouds. For both periods, ice clouds show high peak frequency around 220 K, while water clouds show peak at 300 K. Since most of water clouds satisfy CTT > 227 K, while only 1.3% of water clouds have equal or colder than 227 K of CTTs, CTT ≤ 227 K may be used as a stable criterion for selecting pure ice clouds. Moreover, considering that ice clouds are hardly

warmer than 273 K of CTTs (< 1% of total ice clouds), CTT ≥ 273 K can be used as a water cloud criterion. After determining cloud phase, Mie and Baum scattering models are used for simulating water and ice clouds, respectively. Clouds with CTT between 227 K and 273 K are not used for the simulation because of the difficulty in specifying optical properties of potentially mixed-phase clouds.

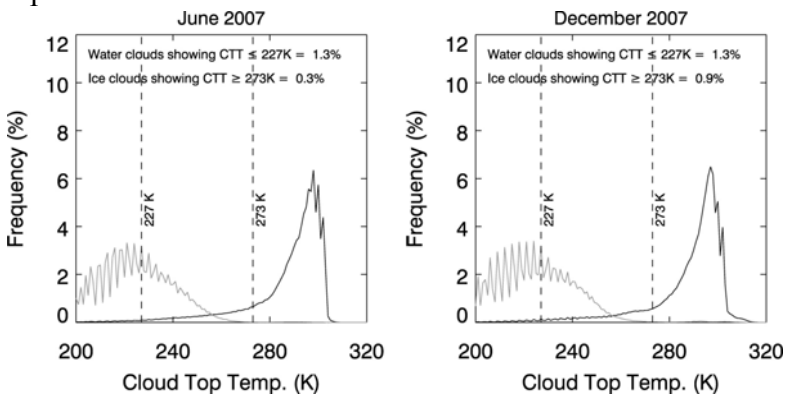

Fig. 3. Frequency distributions of MODIS-derived CTT for water (black solid line) and ice (grey solid line) clouds at a 5-km resolution for June 2007 (left panel) and December 2007 (right panel) over 40°N–40°S, 100°E–180°E area.

7. Effective radius of clouds, which is also produced by the MODIS team, does not have a large impact on reflectances in the visible spectral range but for such an application concerning calibration accuracy it would be recommendable to make use of this quantity. Please comment on this.

We've already used cloud effective radius from MODIS data when applying Method 2. Now it is mentioned.

[Old]
For selected cloud grid targets, sensor-reaching reflectances were simulated using collocated MODIS-derived cloud products.
[New]
For selected cloud grid targets, sensor-reaching reflectances are simulated using collocated MODIS-derived cloud products, such as COT, cloud effective radius, cloud top pressure (CTP), and cloud top temperature (CTT).

8. As for Method 1, a complete description of the RTM and all the input data including radiative transfer solver, ocean BRDF and so on should be given. Furthermore, the choice of the tropical atmospheric profile should be better justified. The ozone absorption band in SEVIRI's 646nm channel has a small influence on the measurement but in the worst case it

can range between 5–10 %, which is also the range of the effect that the authors want to investigate.

Introducing Method 2, all information on the used RTM (SBDART), atmospheric profile (standard tropical profile), surface model (ocean BRDF model), and cloud scattering models (Baum and Mie models) is now provided in the revised version. We agree that variation of atmospheric profiles can introduce simulation errors when fixed tropical profiles are used. Considering that atmospheric profiles should be important when cloud is optically thin and located near surface, we assume the worst case (TOA reflectance is more likely affected by atmospheric profiles) with the smallest COT (= 5) and the low cloud altitude between 1 and 2 km among the possible cloud scenarios. Then we test how TOA reflectances are sensitive to seasonally varying ozone amounts by allowing ±10% of variations of tropical ozone profile [i.e., tropical ozone profile $O_3(z)$, $O_3(z)\times1.1$, $O_3(z)\times0.9$] while other variables are held fixed. Results indicate that up to 0.6% and 0.3% of SEVIRI and MTSAT-1R reflectance can be changed by different ozone profiles, respectively. In addition, we also examine the impact by replacing tropical profile with mid-latitude summer (MLS) profile. It is noted that 1.0% and 1.1% of reflectance differences for SEVIRI and MTSAT-1R visible channels are due to the different atmospheric profiles. These results from the sensitivity test are now included in the revised version.

[Old]

Because the spectral bands of SEVIRI or MTSAT-1R visible channels were located over an insignificant gas absorption band, standard tropical profiles were used to specify the atmospheric conditions. In addition, surface reflectances were specified using the oceanic bidirectional reflectance distribution function (BRDF) model, although we minimized the surface influences by selecting moderately thick cloud targets (COT ≥ 5) over the ocean.

[New]

Because the spectral bands of SEVIRI or MTSAT-1R visible channels are located over an insignificant gas absorption band, standard tropical profile is used to specify the atmospheric conditions. In order to justify the use of standard tropical profile representing the atmospheric status, we conduct a sensitivity test. The use of mid-latitude summer (MLS) profile instead of tropical profile suggests that the change can cause uncertainty in reflectance up to 1% and 1.1% for SEVIRI and MTSAT-1R visible channel when COT = 5, cloud top height = 2 km, and cloud base height = 1 km are used (for a thin and low cloud). Moreover, with the same cloud conditions, we test how TOA reflectances are sensitive to seasonally varying ozone amounts by allowing ±10% of variations of tropical ozone profile [i.e., tropical ozone profile $O_3(z)$, $O_3(z)\times1.1$, $O_3(z)\times0.9$], while other variables are held fixed. Results indicate that up to

0.6% (0.3%) of SEVIRI (MTSAT-1R) reflectance can be changed by different ozone profiles. Relatively small changes in SEVIRI and MTSAT-1R reflectances in sensitivity test justify the use of fixed atmospheric profiles at most within a 1% uncertainty range. In addition, surface reflectances are specified using the oceanic BRDF model that is same to the one used in Method 1, since cloud targets are chosen over the ocean.

9. Method 2 is based on radiative transfer simulations of SEVIRI reflectances starting from optical thicknesses derived from MODIS. Data is collected to 0.5° boxes and compared with measured SEVIRI reflectances averaged over the same box. The step from the high resolution MODIS optical thicknesses to box averages of simulated SEVIRI reflectances is discussed in detail. Two approaches are conceivable: the first one takes the average of the MODIS optical thicknesses over each box and uses it as input for the RTM to compute the SEVIRI reflectances at the box level. The second one first makes a RT computation for every MODIS optical thickness to compute high resolution SEVIRI reflectances and then exploits some sort of averaging procedure to obtain SEVIRI reflectances at the box level. Due to the nonlinear dependence of reflectance on cloud optical thickness, these possibilities produce different results. It is shown that the first procedure produces biases (the PPH bias). The second procedure, where high resolution SEVIRI reflectances are averaged over the entire grid box, is more accurate, but its accuracy also depends on the way how reflectance averages are computed. The authors propose the use of the LN-ICA method (Oreopoulos and Davies, 1998) and show, with the help of an extended MODIS dataset that it is more accurate than the first procedure. At this point two considerations must be made.
1) The first consideration is of general nature and regards the definition of the PPH bias and the method proposed to create simulated SEVIRI box reflectances. One usually wants to derive accurate low resolution (in this case for the grid boxes) reflectances starting from a high resolution spatial distribution of optical thicknesses (τ) making use of a 1D RTM. To this end, the errors produced by the neglect of 3D effects must be assessed. Thus, both 1D and 3D RT calculations for the same cloud field are performed and results compared at the box level. Here, however, the context is slightly different. The τ distribution is derived from space-borne (MODIS) measurements, i.e. each single optical thickness has been derived from a 3D (nature is 3D) reflectance measurement by means of a 1D RT model. Thus, shadowed (dark) cloudy pixels will presumably possess lower τ than in reality while illuminated (bright) cloud sides will probably show too large optical thicknesses. The occurrence and magnitude of these effects depends of course on the given sun-satellite geometry and on the cloud structure itself. Anyway, these optical thicknesses are determined in such a way that a 1D RTM is able to accurately reproduce the (3D) measurements. This means that the authors use an optical thickness field that is affected by 3D effects determined by the MODIS characteristics to first

compute a 1D reflectance field for another satellite sensor with different viewing geometry. I think that this method could produce systematic differences between the simulated SEVIRI reflectances and the measured SEVIRI reflectances because the input optical properties are not the "real" cloud properties in the given boxes, but the cloud properties as observed by MODIS under a given sunsatellite geometry that is different from the geostationary one. Exactly because of 3D radiative effects, systematically higher or lower cloud optical thicknesses could lead to biased SEVIRI reflectances. In order to minimise these effects it is very useful to screen the data in the way the authors do: the use of fully cloudy grid boxes with small internal variability should minimise these problems. However, it is very difficult to say whether this procedure is bias free. Please comment on this.

In this study, for simplifying 3D problems, we divided 3D effects into two parts, i.e. the effects of horizontal inhomogeneity and horizontal radiative interactions. Although these two effects may be closely related to each other, we examined these separately.

We firstly try to quantify the first 3D effects (horizontal inhomogeneity). We agree that realistic cloud field should give more accurate estimation of 3D effects. In many previous studies, *a priori* 3D cloud structure was defined from statistical models or certain observational events (e.g., aircraft), from which ability of 1D simulation was investigated by comparing with 3D simulation results. We expect that observation can give more realistic cloud structures than statistical approaches. However, it is not easy to obtain complete 3D structures from observation, and thus we instead use MODIS-derived 2D cloud field, which uses 1D RTM. As the reviewer pointed out, this cloud field may have different features from reality because of neglecting cloud shadow or illumination. However, the shadow and illumination phenomena are actually the results of second 3D effect (horizontal radiative interaction), and these will be investigated separately in the next part whether the effect produces systematic biases or not. At this point we only focus on the simulation biases caused by ignoring the horizontal inhomogeneity in the grid box, and we assume that MODIS-derived cloud field represents general features of cloud horizontal distribution (2D field) of nature. Moreover, as the reviewer pointed out, the shadow and illumination effects are not included in estimating PPH biases in examination with MODIS data because the same viewing geometry is used in simulation as in the cloud-measured geometry.

As the reviewer suggested, we only use overcast cloud grid boxes and also check sub-grid variability. In those types of clouds, influences of cloud shadow-illumination effects can be minimized when calculating SEVIRI and MTSAT-1R channel reflectances. This is discussed when the second 3D effects are examined. We now mention the limitations of MODIS-measured 2D cloud field, as follows.

[Old]

In this study, to estimate the magnitude of the PPH bias, measured MODIS reflectance data were used along with MODIS cloud products. This is based on the fact that MODIS visible channel reflectances can be accurately calculated with less than 3% uncertainty using cloud parameters of MODIS products on a pixel basis (Ham et al. 2009).

[New]

In this study, to estimate the magnitude of the PPH bias, measured MODIS reflectance data are used along with MODIS cloud products. Note that MODIS-retrieved cloud fields could have certain biases because 1D RTM is used for the retrieval, while cloud shadow and illumination effects are ignored. However, the shadow and illumination effects are actually the results of second 3D effect (horizontal radiative interaction), and this will be investigated separately in the next part whether the effect produces systematic biases or not. At this point we only focus on the simulation biases caused by ignoring horizontal inhomogeneity in the grid box, and we assume that MODIS-derived cloud field represents general features of cloud horizontal distribution (2D field) of nature. Moreover, since observation geometry of COT and viewing geometry of simulation are same, the 3D effects associated with shadow and illumination would be cancelled out.

The estimation of PPH biases is firstly based on the fact that MODIS visible channel reflectances at a pixel point can be accurately calculated within a 3% of uncertainty level using cloud parameters of MODIS products (Ham et al., 2009).

2) The second consideration refers to the example summarised in Table A1. The authors show that the lognormal averaging procedure using simulated high resolution MODIS reflectances produces better agreement with the measured MODIS reflectances averaged over the given grid box than the PPH computation where the averaged MODIS optical thickness over the grid box is used in one RT calculation to derive the MODIS grid box reflectance. First of all, it would be interesting to know how the simpler ICA averaging procedure performs. Second, this MODIS-related example (see Table A1) cannot be directly used to exemplify or support the method proposed. Here, there is no reason for expecting significant deviations between the simulated and the measured MODIS box reflectance. If the MODIS derived optical thickness (1D) can accurately reproduce the MODIS measurements (3D), already and maybe especially the usual ICA average should give accurate coarse MODIS reflectances that are similar to the average of the real MODIS measurements. Furthermore, the bad performance of LN-ICA against PPH in October 2006 and January 2007 should be explained. As far as Fig. A1 and Table A1 are concerned, the authors should specify the details of the MODIS data used, e.g. whether the investigation was at the global scale and how many fully cloud covered grid boxes could be evaluated.

In Table A1 (now Table 1), simulated reflectances from LN-ICA method show better agreements with measured reflectances, in comparison to reflectances from PPH method. This suggests that LN-ICA method well resolves subgrid-scale variations with only few integral points. Please note that the first 3D effect is not cancelled out even though COT-measured geometry and simulation viewing geometry are same. But the second 3D effect associated with the horizontal radiative interaction is cancelled out in this case. Therefore, simulation biases still exist if we consider large-scale simulation but ignore sub-grid variability, as shown in the PPH simulation results. In addition, following the suggestion, we describe how to average subgrid reflectances in the LN-ICA method. Changed paragraph is following:

[New]

After obtaining simplified PDF of COT with an LN function, the grid reflectance can be estimated using Eq. (9). For the efficient integration with relatively small integral points, Gaussian points and weights are employed. Since five Gaussian points produce nearly same integration results as those from eight Gaussian points (not shown), five Gaussian points are employed in this study. Finally, grid reflectances in the LN-ICA method can be obtained as follows:

$$R_{LN-ICA} \simeq \int_{\tau_{\min}}^{\tau_{\max}} R(\tau) p_{LN}(\tau) d\tau \simeq \frac{\tau_{\max} - \tau_{\min}}{2} \sum_{i=1}^{5} w_i p_{LN}(\tau_i) R(\tau_i) \qquad (11)$$

where $\tau_{\min} = E(\tau) - 2\sqrt{V(\tau)}$, $\tau_{\max} = E(\tau) + 2\sqrt{V(\tau)}$, and $\tau_i = \frac{\tau_{\max} - \tau_{\min}}{2} x_i + \frac{\tau_{\max} + \tau_{\min}}{2}$;and x_i and w_i are ith Gaussian point and weight, respectively.

We also discuss why larger simulation errors occur when LN-ICA method is applied for the October 2006 case.

[Old]

When the PPH assumption was used, the monthly means of differences were between +1.1 and 4.6% (the second column of Table A1), while the differences ranged between −2.4 and +0.8% when the LN-ICA method was used (the third column of Table A1). By using the LN-ICA method, most of the positive biases appeared to be removed and there was no dominant sign of simulation biases against the measured reflectances. Therefore, we concluded that the LN-ICA method can be successfully used for removing simulation errors associated with subgrid variation in the large grid (0.5°) calculation.

[New]

When the PPH assumption is used, the monthly means of differences are between +1.1 and 4.6% (the second column of Table 1), while the differences range between −2.4 and +0.8% when the LN-ICA method is used (the third column of Table 1). By using the LN-ICA

method, most of the positive biases appear to be removed and there is no dominant sign of simulation biases against the measured reflectances. In October 2006, slightly larger simulation biases are shown compared to PPH method probably because of the cases that PDFs of observed COTs are irregularly shaped, and thus LN functions cannot fit the original curves of COT PDFs. Except this period, overall magnitude of simulation biases from LN-ICA method is smaller than that from PPH method, suggesting that the LN-ICA method can be successfully used for removing simulation errors associated with subgrid variation in 0.5°-grid calculation.

Used MODIS datasets for examining abilities of PPH and LN-ICA calculations in Fig. A1 (now Fig. 4) are now provided.

[Old]

Using Eq. (A2), PPH biases at the MODIS 0.646-μm channel were estimated for a one-month period (July 2004) and the results were shown in Fig. A1.

[New]

Using Eq. (8), PPH biases at the MODIS 0.646-μm channel are estimated for a one-month period (July 2004) over equatorial Atlantic region (40°W–40°E, 40°N–40°S), and the results are shown in Fig. 4.

Dataset used in Table A1 (now Table 1) is described.

[Old]

To examine how efficiently the LN-ICA method removes PPH bias, the method was applied to an eight-month period of MODIS data.

[New]

To examine how efficiently the LN-ICA method removes PPH bias, the method is applied to an eight-month period of MODIS data over equatorial Atlantic region (40°W–40°E, 40°N–40°S).

10. Again, for the quantification of the ICA error the Monte Carlo model should be referenced and details of the simulations (correlated-k, cloud optical properties...) should be given.

Following reviewer's suggestion, references are provided and RTM input variables are explained in detail.

[Old]

Therefore, the Monte Carlo (House and Avery 1969; Marchuk et al. 1980) RTM was used in this study to quantitatively examine influence of the horizontal radiative interaction. In the

Monte Carlo model, because 3D direction of photon paths can be controlled, both full 3D and ICA modeling are available by turning on and off horizontal photon movements, respectively. Because horizontal photon movements induce horizontal radiative interactions, the ICA bias is defined as the difference between ICA and full 3D modeling results (Cahalan et al. 1994b); that is:

$$\Delta R_{ICA} = R_{ICA} - R_{3D} \qquad \text{(A5)}$$

where ΔR_{ICA} is ICA bias; and R_{ICA} and R_{3D} are simulated reflectances from ICA and full 3D methods, respectively. The ICA bias is estimated only for nadir view (VZA = 0°) because horizontal photon movements produce horizontal shift of cloud image for slanted view (VZA > 0°), and in this case direct comparison is not possible between ICA and 3D simulation results.

[New]

Therefore, the Monte Carlo (House and Avery 1969; Marchuk et al. 1980) approach is considered in this study to quantitatively examine influence of the horizontal radiative interaction. The Monte Carlo model generates several numbers of photons in 3D domain and simulates scattering and absorption events for each photon. In this study we use GRIMALDI (Scheirer and Macke, 2003) Monte Carlo model, and consider 100,000 photons × total column number in the domain. In this study, the total column number is defined as the number of CloudSat pixels. Since the horizontal photon movement induces horizontal radiative interactions, both full 3D and ICA modeling are available by turning on or off the horizontal movement option that is available in GRIMALDI. Then ICA bias is defined as the difference between ICA and full 3D modeling result (Cahalan et al. 1994b), i.e.:

$$\Delta R_{ICA} = R_{ICA} - R_{3D} \qquad \text{(A5)}$$

where ΔR_{ICA} is the ICA bias; and R_{ICA} and R_{3D} are simulated reflectances from ICA and full 3D method, respectively. The ICA bias is estimated only for nadir view (VZA = 0°) because horizontal photon movement produces a horizontal shift of cloud image for slanted view (VZA > 0°), and in this case direct comparison is not possible between ICA and 3D simulation results.

As boundary conditions, Lambertian surface is assumed with albedo of 0.05, while a periodic condition is assumed at the side boundaries. In the calculation domain, only clouds are regarded as extinction media, while no aerosol and gas are assumed. Because of the ignored gas absorption and nearly same cloud properties over the visible spectrum band in interest, the simulation results show a small spectral dependence. Therefore, fixed wavelength of 0.646 μm is used in the calculation, expecting similar results to SEVIRI or MTSAT-1R visible channels. In addition, even if we expect changes in the overall magnitude

of cloud reflectance when different cloud phase or particle effective radius are used, the effect of horizontal interactions such as photon leakages and illumination-shadow contrasts appears to be very small. Therefore cloud phase is fixed to be ice; particle size is assumed to be 20 μm.

Scheirer, R., and Macke, A.: Cloud-inhomogeneity and broadband solar fluxes, *J. Geophys. Res.,* **108,** 4599, doi:10.1029/2002JD003321, 2003.

11. A justification for the choice of the extinction coefficient value of 0.005m−1 is also expected: is this a typical value?

Following the suggestion we added reasons of choosing the fixed value.

[Old]

For the given cloud structure, a fixed extinction coefficient of 0.005 m^{-1} was used to calculate the total columnar COT between cloud top and base heights. Calculated COTs were between 0 and 80, which are within the typical range of MODIS-derived COTs.

[New]

For the given cloud structure, a fixed extinction coefficient of 0.005 m^{-1} is used to calculate the total columnar COT between cloud top and base heights. The extinction coefficient of 0.005 m^{-1} is not based upon measurements but is arbitrarily chosen. However, COT simulations with CloudSat-derived cloud top and bottom and a fixed extinction coefficient of 0.005 m^{-1} are able to produce COTs in the range of 0–80, which are in the typical range of MODIS COT measurements. Therefore, we think that the use of fixed coefficient of 0.005 m^{-1} may produce plausible COT fields from which 3-D effects can be studied. In addition, many studies pointed out that cloud morphology gives much larger influences on ICA biases, compared to extinction variation in the cloud layer (Loeb et al. 1998; Marshak et al. 1998; Varnai and Davies 1999; Varnai 2000). Therefore, a fixed extinction coefficient is used to examine general features of ICA biases, while cloud shape is described from satellite measurements.

12. The extension of 2D profiles to 3D profiles should be explained in more detail.

Now extension of 2D profiles to 3D profiles is more clarified.

[Old]

CloudSat 2B-GEOPROF data provide two-dimensional vertical cross-section images of clouds along satellite paths (*x* axis) with a 1.1-km resolution. Therefore, homogeneous conditions were assumed to construct 3D cloud structures in the model domain by

considering a perpendicular axis (*y* axis) to the satellite track.

[New]

CloudSat 2B-GEOPROF data provide two-dimensional (2D) images of the vertical cross-section of clouds along satellite paths with a vertical resolution of 240 m and a horizontal resolution of 1.1 km. To construct the 3D cloud structures from observed 2D profiles, the 2D profile is extended infinitely along a cross-track direction. Thus variation of cloud structure is not allowed along the cross-track direction.

13. According to Fig. A2 it seems that the authors mainly simulated clouds with iced tops while Method 2 mainly refers to water clouds, at least as far as SEVIRI is concerned. Does this affect the evaluation of the ICA error?

As also discussed in #10, the choice of cloud phase can increase or decrease overall magnitude of reflectance, but noticeable changes in horizontal interactions are not found from the choice of cloud phase. Figure D2 represents ICA biases for water cloud. Comparing to the ice cloud results in Fig. A3, (now Fig. 6), ICA biases are not much discernible.

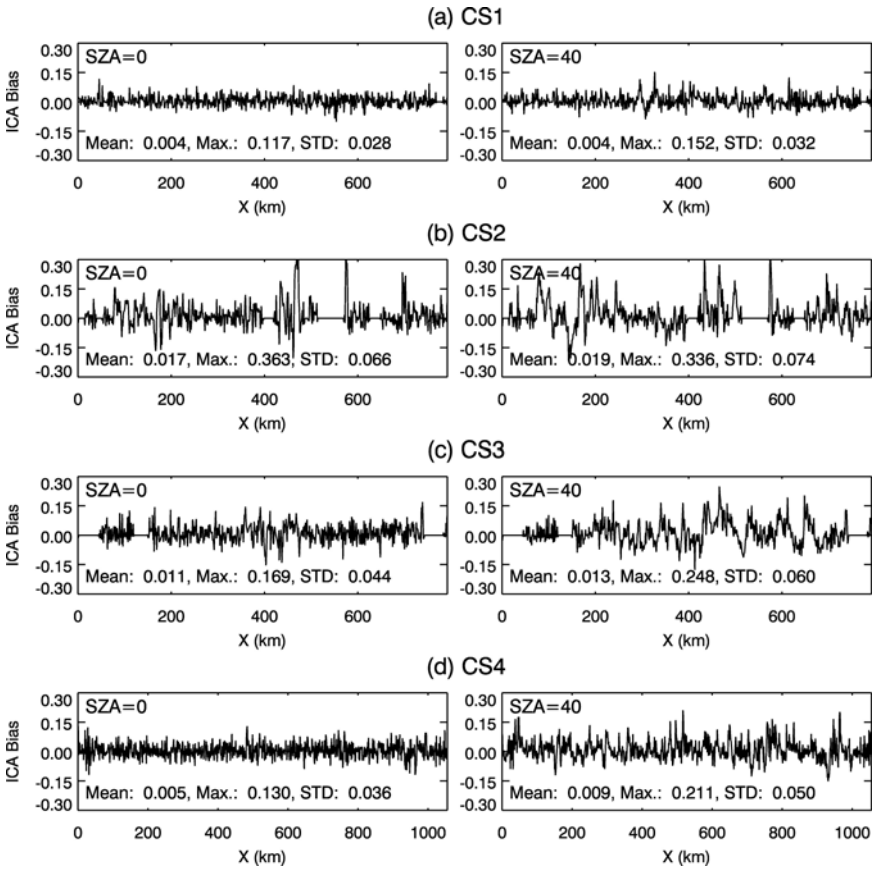

Figure. D2. Same as Fig. 6 but for water cloud.

14. It is also stated that the ICA bias represents a random noise that can be reduced by averaging over time or space. This contradicts also Zinner et al. (2006, Fig. 9a) where depending on cloud cover the ICA bias is plotted. Please check or explain results concerning this issue.

Zinner et al. (2006) proposed a novel method to calculate 3D cloud structures from high-resolution (15 m × 15 m) radiance observations. In this paper, reflectances from ICA and 3D simulations are compared by means of power spectrums. For example, smoothing effects generated by horizontal photon leakages decrease amplitude of high frequency in 3D simulation results, in comparison to ICA results. On the contrary, sharpening effects induced by shadowing and illuminating phenomena increase amplitude of high frequency in 3D simulation results. In Figs. 3–5 of Zinner et al. (2006), different power spectrums are obtained between ICA and 3D simulations, even though same cloud field is used for the simulation. However, different amplitudes of power spectrum do not necessarily mean systematic differences of reflectances between two simulation methods, while the different amplitude represents the different degree of fluctuation in the simulated reflectances. Instead the close agreement in amplitudes at low frequency suggests that ICA and 3D simulation results are close to each other in the large scale aspect. Meanwhile, many other studies suggest that PPH biases have positive signs (e.g., Cahalan et al. 1994a; Oreopoulos and Davies 1998a; Pincus et al., 1999), while ICA biases have both positive and negative signs that are minimized in large-scale simulation under small SZA for overcast clouds (e.g., Marshak et al., 1995; Varnai, 1998). All these suggest that ICA biases are removed from spatial or temporal average, consistent with those found from this study.

Cahalan, R. F., Ridgway, W., Wiscombe, W. J., Bell, T. L., and Snider, J. B.: The albedo of fractal stratocumulus clouds, J. Atmos. Sci., 51, 2434–2455, 1994a.

Marshak, A., Davis, A., Wiscombe, W., and Cahalan, R.: Radiative smoothing in fractal clouds, J. Geophys. Res., 100, 26 247– 26 261, 1995.

Oreopoulos, L., and Davies, R.: Plane parallel albedo biases from satellite observations. Part I: Dependence on resolution and other factors, J. Climate, 11, 919–932, 1998a.

Pincus, R., McFarlane, S. A., and Klein, S. A.: Albedo bias and the horizontal variability of clouds in subtropical marine boundary layers: Observations from ships and satellites, J. Geophys. Res., 104, 6183–6191, 1999.

Varnai, T.: Influence of three-dimensional effects on the spatial distribution of shortwave cloud reflection, J. Atmos. Sci., 57, 216–229, 1998.

Zinner, T., Mayer, B., and Schröder, M.: Determination of 3D cloud structures from high resolution radiance data, Journal of Geophysical Research, 111, doi:10.1029/2005JD006

062, 2006.

15. A posteriori, looking for instance at Fig. 2, a very similar performance of Method 1 and Method 2 is observed which seems to confirm that the conditions used in Method 2 to minimise 3D effects (both in the MODIS retrieval and in the RT simulations) were effective. However, it should be stated that Method 1 and Method 2 are related to each other because cloud properties input to the RTM have been derived from the reflectance measurements that are used in Method 1 to find collocations. Ham et al. (2009) show for instance that detailed 1D RT calculations are able to reproduce the MODIS shortwave band reflectances with an uncertainty of 5%. However, the computations in this paper could not be as accurate as those in Ham et al. (2009), because ancillary information (like atmospheric profiles) are missing, such that one could expect a similar or worse accuracy than for Method 1. Thus, the benefits and characteristics of this method should be clearly stated and emphasised with respect to Method 1. Possible characteristics of Method 2 can be the fact that it only considers areas with homogenous and complete cloud coverage. Furthermore, this method enables to take into account the different spectral response functions in a more detailed way than in Method 1.

A new paragraph is added in the revised version.

[New]

Although the performance of Methods 1 and 2 can be related to each other because cloud products are from same MODIS radiances, the Method 2 appears to have its own advantages. Note that Method 2 has fewer restrictions in choosing the spectral region for channels because the radiative transfer modeling proposed in this study incorporates any shape of SRFs. Moreover, water or ice cloud properties within the given spectral band can be easily obtained from Mie calculation or Baum's hyperspectral data (2005a, b, and 2007), respectively. Compared to Method 1, Method 2 is a novel approach because comparison between two channels is feasible only if strong gas absorption is avoided and two channels are located in the similar spectral region. In this study, a simple tropical profile is used for the RT simulations since SRFs of Meteosat-8/9 and MTSAT-1R visible channels are located in the negligible gas absorption band. However, information on atmospheric profiles such as AIRS profiles can certainly improve the accuracy of Method 2 in particular for the channels whose SRF is located over the strong gas absorption band.

Baum, B. A., Yang, P., Nasiri, S. L., Heidinger, A. K., Heymsfield, A. J., and Li, J.: Bulk scattering properties for the remote sensing of ice clouds. Part 3: High resolution spectral models from 100 to 3250 cm^{-1}, J. Appl. Meteor. Clim., 46, 423–434, 2007.

Also added is the sentence in Summary, stating that Methods 1 and 2 are related to each other, i.e.:

[Old]

Suggested measurement biases of Meteosat-8/9 and MTSAT-1R visible channels from cloud target simulations were consistent with results from the ray-matching technique.

[New]

Suggested biases in Meteosat-8/9 and MTSAT-1R visible channel calibration appear to be consistent with results from the ray-matching technique since regression results from two methods are mostly overlapped. This implies that 3D effects are effectively taken into account in the LN-ICA method because the LN-ICA method gives consistent results with results derived from MODIS radiance observations. However, it is also should be noted that performances of Methods 1 and 2 can be related to each other since cloud products used for Method 2 are from the same radiances used for Method 1.

16. The discussion of 3D effects and possible measures to minimise them is an important topic that is rightly pointed to in the manuscript. In this context, the plane-parallel error (PPH) and the ICA error are discussed, mainly in Appendix A. Because it represents an important aspect of the method, this discussion should be moved forward to Sect. 2.2 under consideration of the above comments.

Following reviewer's suggestion, Appendix is moved into the section 2.2.

Method 3

17. The authors cite Sohn et al. (2009) where the DCC detection applied to MODIS is explained. Adaptation of this method to SEVIRI and MTSAT-1R is presented, but it is not clear whether the same threshold values are applied to all three sensors. Please specify.

Same thresholds are applied for homogeneity checks of SEVIRI and MTSAT-1R. A new sentence is added to clarify this.

[New]

Note that same thresholds (i.e., 1 K for STD of TB_{11} and 0.03 for STD of visible reflectance normalized by its mean) are applied for the homogeneity checks despite different numbers of surrounding pixels used for calculating the STD.

18. Furthermore, it should be pointed out that MODIS is not used here at all. As for Method 2 and Method 1, more details about the RT calculations should be given.

More detailed explanation is found in the revised version.

[Old]

Once DCC targets were selected, cloud parameters were assumed for the radiative transfer simulation of DCC targets (COT=200 and effective radius=20 μm). Sohn et al. (2009) demonstrated that the simulations of the visible channel reflectance for the DCC targets can be achieved within an uncertainty of 5% using these conditions.

[New]

Once DCC targets are selected, ice cloud phase is assumed since the uppermost part of clouds overshooting the TTL mostly contains nonspherical ice particles. In addition, for the radiative transfer simulation for DCCs, their COT and effective radius are assumed to be 200 and 20 μm, respectively. It is noteworthy to emphasize that MODIS data are not used in Method 3 at all, although *a priori* conditions of COT and effective radius based on MODIS observations are used for the simulation (Sohn et al., 2009). In addition, cloud altitude is assumed to be located between 1 km and 15 km, based on the fact that overshooting clouds are thicker than 10 km (Chung et al., 2008; Luo et al. 2008). Expecting insignificant influence of the atmosphere and surface on the DCC simulation, standard tropical atmospheric profiles and oceanic BRDF model are used, same as in Methods 1 and 2. Note that DCC targets are collected regardless of the land surface types, even though the oceanic BRDF model is used for the calculation of surface reflectance. Sohn et al. (2009) demonstrated that visible channel simulations can be achieved within an uncertainty of 5% using these fixed RTM conditions over DCC targets.

Chung, E.-S., Sohn, B. J., and Schmetz, J.: CloudSat shedding new light on high-reaching tropical deep convection observed with Meteosat, Geophys. Res. Lett., 35, L02814, doi:10.1029/2007GL032516, 2008.

Luo, Z., Liu, G. Y., and Stephens, G. L.: CloudSat adding new insight into tropical penetrating convection. Geophys. Res. Lett., 35, L19819, doi:10.1029/2008GL035330, 2008.

19. All considerations related to 3D effects as well as all measures used to minimise them should be provided in this Section (Sect. 2.3) and not postponed to the Appendix.

Following the suggestion, discussion related to 3D effects in Method 3 is moved to section 2.3.

[New]

The SBDART RTM implemented with 20 streams is used to calculate the visible channel reflectances of DCC targets, which may result in simulation biases by 3D effects similar to

Method 2. As demonstrated in section 2.2, PPH bias is produced by a nonlinear relationship between COT and reflectance. However, considering that the nonlinearity of reflectance mostly vanishes in the range of COT > 100, the PPH assumption appears to introduce only minor errors in the DCC simulation. Moreover, DCC targets of SEVIRI and MTSAT-1R are smaller than 0.05°; therefore, PPH biases are negligible once homogeneous targets are chosen (see Fig. 4). The homogeneity conditions of $STD(R_{0.6})/Mean(R_{0.6}) \leq 0.03$ and $STD(TB_{11}) \leq 1$ K certainly help choosing those types of clouds. ICA biases may also influence DCC calibration results; however, ICA biases can be effectively minimized by temporal averaging, homogeneity checks with STD of visible reflectances and TB_{11}, and the use of overcast clouds under relatively smaller SZAs (≤ 40°). In this study, daily averaging is performed only if the number of selected DCC targets is greater than 10 per day.

Application of the Methods

20. For all methods proposed in the paper four or seven months of data were used to assess inter-calibration differences between SEVIRI and MODIS and MTSAT-1R and MODIS. First of all it should be explicitly mentioned in the text how many targets could be used in each method. Furthermore, and most importantly, the given months should be separated. Of course, enough targets must be still available to obtain statistically significant results. If this is not possible with one month, then two consecutive months could be considered. The point is that due to sensor degradation (as explained in the manuscript) calibration accuracy could change with time. Mixing up different months from different years increases the chance that measurements with different calibration accuracy are used. As far as both Method 1 and Method 2 are concerned, I recommend to consider Terra and Aqua separately. Although both have a radiometric accuracy of ≤2 %, they can still have different calibrations inside this range.

We think the reviewer's request to separate the results into Terra and Aqua is valid. Before considering temporal changes, we examined differences between results from Terra and Aqua in Method 1 (Fig. D3). In Fig. D3, much smaller targets are available for Aqua-Meteosat collocations compared to Terra-Meteosat collocations. This is because of different viewing angles of Terra and Aqua in the ray-matching process caused by different satellite paths (descending for Terra and ascending for Aqua). Despite of different numbers of used targets and 2% of calibration differences (Minnis et al., 2008) between Terra and Aqua visible sensors, results of SEVIRI visible channels using Terra and Aqua satellites are not much discernible from each other in Fig. D3. Different regression equations are derived from Terra and Aqua, but points in scatter plots seem to be located with similar degrees of biases. Therefore, it is concluded that the differences between Terra and Aqua appear to be

insignificant, in comparison to uncertainties shown in each scatter diagram.

In Method 2, we expect that impacts of calibration differences between two MODIS sensors are relatively small in the results because Method 2 does not use measured MODIS reflectances directly, while retrieved cloud products are used for the simulation. Of course the simulation results should not be free from calibration differences of two MODIS sensors because MODIS COT and effective radius are obtained from measured reflectances. In Fig. D4, calibration results of Meteosat-8/9 visible channels from Method 2 are separately displayed with respect to Terra and Aqua. Despite of different cloud characteristics obtained from Terra and Aqua, the differences in results from Terra and Aqua appear to be small, compared to the degree of scatterings in each diagram. Therefore, we decided to represent temporal changes of calibration results without separating into Terra and Aqua. We added the following statement in section 3.1.

[New]

Note that results of Methods 1 and 2 are not displayed separately for Terra and Aqua MODIS. It is because differences between Terra and Aqua are considered to be small compared to the degree of uncertainties of each method, although about 2% differences between Terra and MODIS can be expected (Minnis et al., 2008).

Minnis, P., Doelling, D., Nguyen, L., Miller, W., and Chakrapani, V.: Assessment of the visible channel calibrations of the VIRS on TRMM and MODIS on Aqua and Terra, *J. Atmos. Oceanic Technol.*, **25,** 385–400 , 2008.

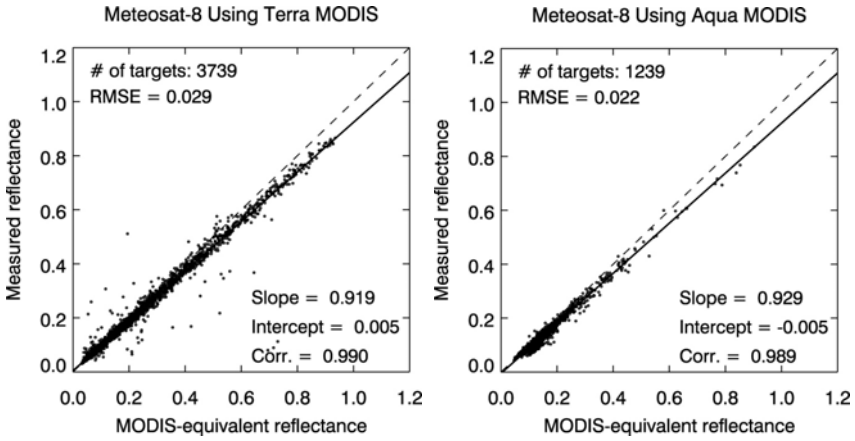

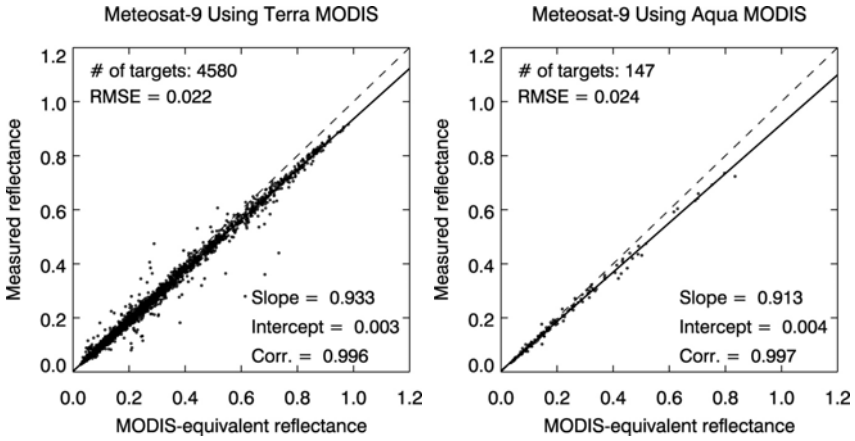

Figure D3. Calibration results of Metoesat-8/9 0.640-μm channels from Method 1. The results are separately represented for Terra and Aqua MODIS sensors.

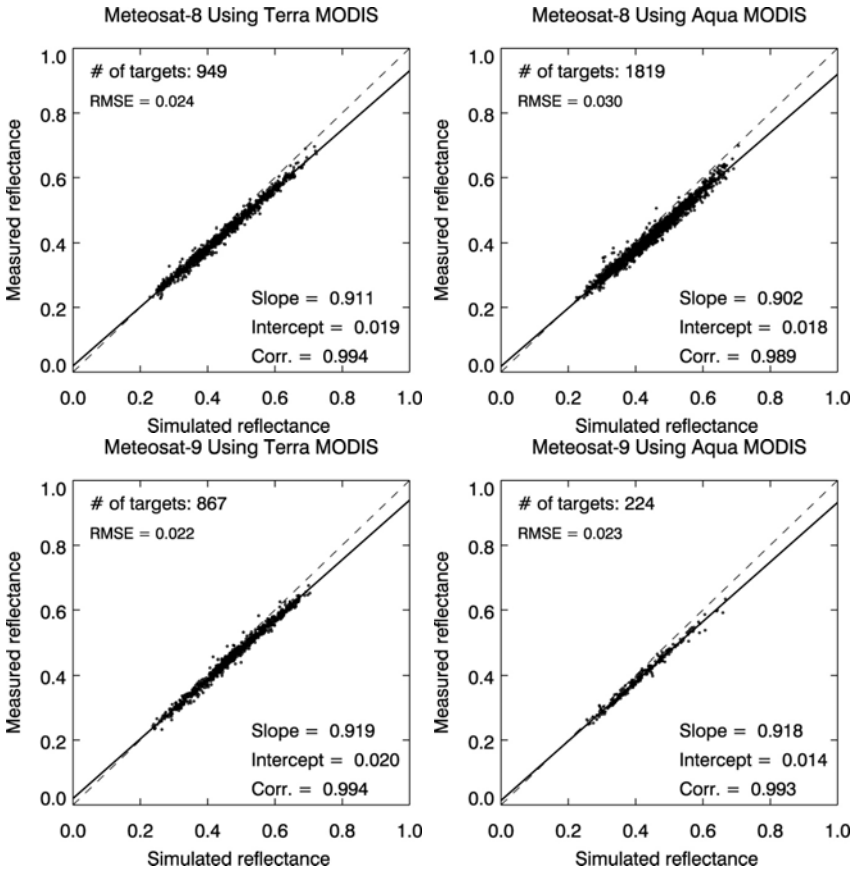

Figure D4. Calibration results of Metoesat-8/9 0.640-μm channels from Method 2. The results are separately represented for Terra and Aqua MODIS sensors.

By separating calibration results for each month, we change results of this paper. In addition, the number of used calibration targets is given in scatter diagram. Changed parts are following.

[New]

3. Results

3.1. Meteosat-8/9 SEVIRI 0.640-μm visible channels

The measurements of SEVIRI 0.640-μm channels aboard Meteosat-8 and -9 are compared against MODIS 0.646-μm channel measurements by applying Method 1. MODIS-equivalent SEVIRI 0.640-μm channel reflectances are obtained by applying Eqs. (1)−(4). Regardless of the season, all collocated targets are selected from the area of 40°W–40°E, 20°N–20°S, satisfying smaller SZA (≤ 40°), VZA (≤ 40°) and imposed conditions for the ray-matching. In Fig. 7, comparison is made for each month between measured SEVIRI and MODIS-equivalent SEVIRI reflectances. Their associated regression lines are presented as black solid lines, and corresponding regression statistics and the number of used targets are given in the plots. The number of chosen targets is greater than 1000 for each month and scattered patterns generally cover most of reflectances ranging from 0 to 1. The regression slopes are between 0.894 and 0.936 for Meteosat-8 (four upper panels of Fig. 7) and between 0.925 and 0.939 for Meteosat-9 (four bottom panels of Fig. 7), while intercepts are nearly zero (< 0.01) for both Meteosat-8 and Meteosat-9. No significant difference is noted between Meteosat-8 and Meteosat-9. Obtained regression slopes except for July 2004 are in the range of 0.93–0.94 with near zero intercepts, corresponding to 6–7% of low bias of SEVIRI measurements against MODIS measurements.

The calibration results of Meteosat-8/9 visible channels from Method 1 are quite similar to the results from other previous studies based on the ray-matching technique. Doelling et al. (2004) showed that MODIS 0.646-μm channel radiances are shown to be 8% larger than Metoesat-8 0.640-μm channel radiances. In addition, Jan Fokke Meirink at KNMI (personal communication, 2009) compares SEVIRI and MODIS visible channels after the atmospheric correction, showing MODIS 0.646-μm channel reflectances 7% (6%) larger than Meteosat-8 (Meteosat-9) 0.640-μm channel reflectances. All these results commonly assert low measurement biases of SEVIRI 0.640-μm channels, implying that the operational calibration of Meteosat visible channels using ocean and desert targets (Govaerts et al., 2004) may underestimate the visible channel reflectance.

Meteosat-8/9 SEVIRI 0.640-μm channel reflectances are simulated using MODIS cloud products as inputs to an RTM, and these serve as references for examining SEVIRI 0.640-μm channel measurements (Method 2). In the simulation, only water cloud targets are used to minimize simulation errors associated with nonspherical cloud particles. In Fig. 8, comparisons are made between simulated and measured SEVIRI 0.640-μm channel reflectances for each month. Because of the applied threshold of COT ≥ 5 for selecting cloud-only targets, reflectances smaller than 0.2 are not present in the plots. In general, the selected target numbers are smaller than those used in Method 1 and larger temporal variations in the numbers are evident (e.g., as a worst case only 29 targets are available

during April 2007). In Fig. 8, regression lines are given as black solid lines and associated statistics are provided. Regression slopes are between 0.880 and 0.909 for Meteosat-8 (four upper panels of Fig. 8), and between 0.912 and 0.940 for Meteosat-9 (four bottom panels of Fig. 8), while regression intercepts are around 0.02 for both satellites. Regression slopes for Meteosat-8 are generally smaller than those for Meteosat-9, but the differences are not statistically confident because of insufficient cloud targets for certain months (e.g., July 2004, January 2007, and April 2007). In Fig. 8, regression lines from Method 1 are also given as grey solid lines for comparing with Method 2 (black solid lines). Although Method 2 generally produces smaller slopes and larger intercepts than Method 1 for overall periods, black and grey lines are mostly overlaid with each other. Decreased slopes in Method 2 seem to be counterbalanced with increased intercepts. Therefore, it is concluded that Method 2 also provides a similar degree (6–7%) of low measurement biases of Meteosat-8 and Meteosat-9 0.640-μm channels, in comparison to MODIS measurements. Slight differences in regression results between Methods 1 and 2 are likely due to the target reflectances larger than about 0.2 in Method 2, causing larger uncertainties in the regression intercepts. Note that results of Methods 1 and 2 are not displayed separately for Terra and Aqua MODIS. It is because differences between Terra and Aqua are considered to be small compared to the degree of uncertainties of each method, although about 2% differences between Terra and MODIS can be expected (Minnis et al., 2008).

DCC targets are selected using SEVIRI window channel measurements, and the reference reflectances for those selected DCC targets are produced from simulations with characteristic cloud optical properties (Method 3). We found a bundle of points situated over the simulated reflectance around 1, hindering the linear regression between simulated and measured SEVIRI reflectances. Instead monthly frequency histograms of relative differences [(measured – simulated)/simulated × 100%] are provided in Fig. 9. High peaks in frequency are appeared at similar reflectance values throughout all periods. Monthly means of the relative differences are from –9.1% to –8.6% for Meteosat-8 (left panel of Fig. 9), and from –9.0% to –7.4% for Meteosat-9 (right panel of Fig. 9), implying low measurement biases of SEVIRI 0.640-μm channels. In comparison to Method 1 or Method 2 showing 6–7% of low biases, the degree of biases from Method 3 appears slightly stronger. For the quantitative comparison amongst three methods, we apply regression equations obtained in Method 1 and 2 to predict measurement biases at the MODIS-equivalent reflectance around 1 where DCC targets are located. Measurement biases of –7.8% and –6.5% are predicted from Method 1 for Meteosat-8 and Meteosat-9 DCC targets, respectively. On the other hand, –7.7% and –5.9% of measurement biases are predicted from Method 2. These predicted biases are displayed with vertical lines in Fig. 9. It is certain that Method 3 produces systematically larger biases by 2–3%, in comparison to results from Method 1 or 2.

In Fig. 10, results from Method 3 are directly compared with results from Methods 1 and 2. Monthly regression lines from Methods 1 and 2 (shown in Figs. 7 and 8) are given as grey and black solid lines, respectively, while Method 3 results are given with crosses. Each cross in Method 3 results represents a daily average. As shown in Fig. 9, crosses are below the two regression lines, the discrepancy of the DCC results from Methods 1 and 2 appears to be evident with orders of 2–3%. In Sohn et al. (2009), the accuracy of Method 3 is shown to be within a 5% uncertainty level, and therefore discrepancy of Method 3 from Method 1 or 2 may be attributed to uncertainties in Method 3. However, considering that simulations by the DCC method (Method 3) did not show an apparent bias when applied to the well-calibrated MODIS visible channel (Sohn et al. 2009), the discrepancy of Method 3 may be interpreted as the saturation characteristics of SEVIRI visible channels when targets are highly reflective (Yves Govearts at EUMETSAT, personal communication, 2010). Similar saturation characteristics can also be inferred from the inter-satellite calibration results of Jan Fokke Meirink at KNMI (personal communication, 2009), which shows larger biases of Meteosat-8/9 measurements at the high reflectance end. However, a more detailed explanation appears to be beyond the current research scope and thus deserves a separate examination.

3.2. MTSAT-1R visible channel

MTSAT-1R 0.724-μm channel measurements are compared to MODIS 0.646-μm channel measurements using the ray-matching technique (Method 1). Throughout the seven-month period, all collocated targets are shown to be located in the area of 100°E–180°E, 20°N–20°S. For the chosen targets, measured MODIS channel reflectances are converted to MODIS-equivalent MTSAT-1R reflectances using Eqs. (5) and (6), and these converted MODIS-equivalent reflectances are compared with measured MTSAT-1R reflectances (Fig. 11). In comparison to the SEVIRI results (Fig. 7), the MTSAT-1R 0.724-μm channel exhibits a more scattered pattern. This is probably due to the scan method of JAMI (David R. Doelling of NASA Langley, personal communication, 2010). Moreover, if MTSAT-1R wobbles from the nominal position (140°E, 0°N), then the viewing geometry at each pixel point is correspondingly changed from the nominal value, causing uncertainties in the ray-matching process. On a monthly basis, linear regression results in slopes between 0.777 and 0.802, and intercepts between 0.015 and 0.037. The slopes are much smaller than 1. Furthermore, intercept off the zero causes the calibration uncertainty depending on the magnitude of reflectance. Bias should be much smaller when reflectance is small, for example in case of reflectance < 0.3. In contrast, underestimate of calibrated reflectance becomes worse when the reflectance becomes larger, resulting in about 20% of underestimate at the high end of MODIS-equivalent reflectance.

MTSAT-1R 0.724-μm channel reflectances are simulated with MODIS cloud products, and the simulation results are used to examine MTSAT-1R measurements (Method 2). Since low

cloud occurrences are not frequent enough for the calibration in the analysis domain (100°E–180°E, 40°N–40°S), abundant high cloud targets containing ice cloud particles are included in the Method 2 analysis. In the process, more than 300 calibration targets are collected for each month. Compared to Meteosat-8/9 results (Fig. 8), a larger degree of scatterings is noted between simulated and measured reflectances -- Fig. 12. Again, this may be due to scan problems of MTSAT-1R as well as simulation uncertainties of ice cloud targets related to nonspherical habits. In spite of the large scattering, measured reflectances are linearly correlated with simulated reflectances, showing regression slopes of 0.742–0.799, and intercepts of 0.033–0.059. These results are consistent with those obtained from Method 1, showing a near agreement between two regression lines (i.e. grey line vs. black line shown in each diagram of Fig. 12). Therefore, Method 2 also suggests an underestimate of calibrated reflectance up to 20% at the high end of reflectance and incorrect space count offset of the MTSAT-1R calibration.

These results are consistent with Okuyama (2009) results based on ocean-desert-cloud combined targets in which the regression slope between simulated and measured reflectances was around 0.8. However, Okuyama (2009) showed a near zero intercept offset, significantly different from offset results from both Method 1 and Method 2, probably because of more uncertain parameterization of dark ocean targets.

MTSAT-1R visible channel reflectances simulated over DCC targets using Method 3 are compared with measured reflectances. Monthly frequency distributions of the relative differences of measured reflectances are plotted against simulation results in Fig. 13 [(measured – simulated)/simulated × 100%]. Although much broader frequency distributions are found compared to SEVIRI visible channels (Fig. 9), their peaks are appeared at similar reflectances over the analysis period, suggesting that results are not much variant over the time. Resultant monthly mean differences ranging from –19.8% to –17.0% are in line with biases predicted from Methods 1 and 2; MTSAT-1R measurement biases at reflectance at 1 were calculated to be –18.3% and –18.7% from Methods 1 and 2, respectively -- find seven month mean biases expressed as vertical grey and black lines in Fig. 13. Differences should be small amongst Methods 1, 2, and 3 because the mean position of high peaks of histograms is located near the vertical grey and black lines.

In Fig. 14, results from Method 3 are compared with those from Methods 1 and 2 using scatter plots. Again results indicate that DCC results are in near agreement with what predicted from two regression results, suggesting the measurement biases of MTSAT-1R visible channel to be between –19.5% and –16.7% around a unit reflectance. The consistency found amongst MTSAT-1R results from Methods 1, 2, and 3 strongly suggests that the 2% of underestimate of reflectance by the Method 3 for the SEVIRI visible channels should not be due to the deficiency of Method 3, but due to the saturation of the sensor capability of

detecting the high side of reflectance. Furthermore, it is suggested that the large scattered patterns found in MTSAT-1R results from Methods 1 and 2 (two or three times larger than RMSEs of Meteosat-8/9) are not likely due to the water vapor absorption around 0.724 μm. It is because the DCC results showing the same degree of scattering should not be sensitive to the water vapor absorption, as seen in the comparison between Fig. 10 and Fig. 14.

4. Summary

In this paper we examined the performance of operational calibration of Meteosat-8/9 SEVIRI 0.640-μm and MTSAT-1R 0.724-μm visible channels using three calibration methods. The first method is based on the ray-matching technique for inter-satellite calibration. MODIS 0.646-μm channel is used as a reference, and reflectances are compared between MODIS and SEVIRI, and MODIS and MTSAT-1R only over oceanic regions. Regression equations are obtained from radiative transfer simulations to convert measured MODIS reflectances into MODIS-equivalent SEVIRI or MTSAT-1R channel reflectances. The results obtained from the ray-matching technique indicate that SEVIRI calibration coefficient is biased low by 6–7%. On the other hand, MTSAT-1R calibration errors appear to vary with the magnitude of reflectance itself because of the incorrect space offset count; a positive bias near zero reflectance turns into negative bias up to –20% in case of reflectance around 1.0.

The Meteosat-8/9 and MTSAT-1R channel reflectances are simulated using collocated MODIS cloud products, such as COT, particle effective radius, CTT, and CTP as inputs for the radiative transfer model. In the simulation, the LN-ICA method (Oreopoulos and Davies 1998b) is adopted to describe the subgrid variability because the plane-parallel assumption at each grid box could generate simulation errors by 3D radiative effects. Horizontal radiative interaction appears to be negligible as a result of 0.5°-grid spatial averaging, homogeneity checks [$STD(R_{0.6}) \leq 0.1$], and the use of moderate SZAs ($\leq 40°$). Suggested biases in Meteosat-8/9 and MTSAT-1R visible channel calibration appear to be consistent with results from the ray-matching technique since regression results from two methods are mostly overlapped. This implies that 3D effects are effectively taken into account in the LN-ICA method because the LN-ICA method gives consistent results with results derived from MODIS radiance measurements. However, it is also should be noted that performances of Methods 1 and 2 can be related to each other since cloud products used for Method 2 are from same radiances used for Method 1.

Results from these two methods are compared with those derived from the DCC method. It is suggested that Meteosat-8/9 measurements may not be sensitive enough to discretize the reflectance when targets are highly reflective, suggesting a saturation of measured radiances. In contrast, there is no particular pattern showing the saturation for the MTSAT-1R visible channel as shown in two regression lines going through a bundle of DCC-derived points.

Overall, all three calibration methods show an agreement within 2–3% and suggest that the current Meteosat-8/-9 SEVIRI 0.640-μm channels underestimate reflectances by 6–9%. It is also noted that the current MTSAT-1R visible sensor may be subject to biases, depending on the reflectance ranging from +5% at near 0.1 to −20% at near 1.0. Further study is required to examine why the MTSAT-1R shows a diverse error range depending on the target reflectance.

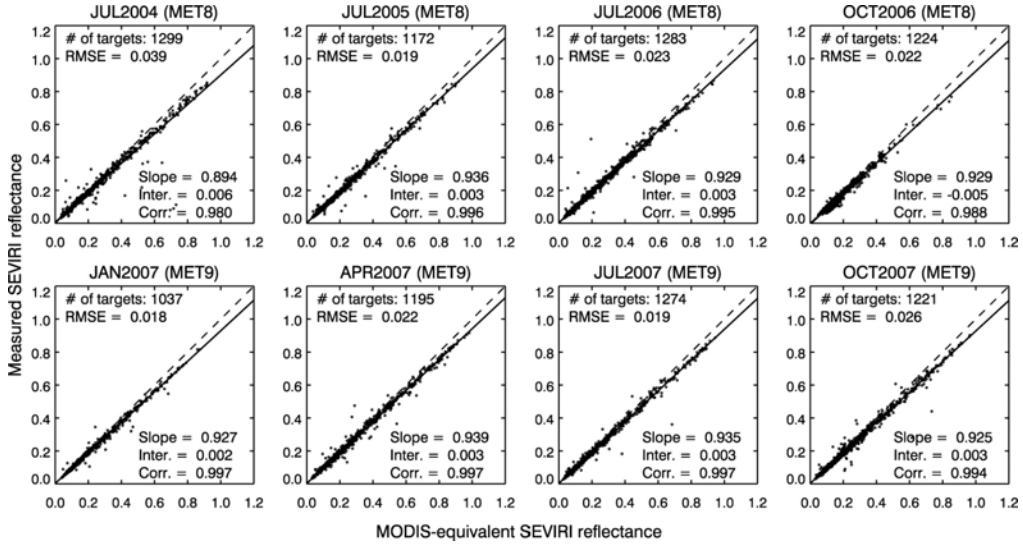

Fig. 7. Scatter plots of MODIS-equivalent SEVIRI vs. measured SEVIRI 0.640-μm channel reflectances of (top) Meteosat-8 and (bottom) Meteosat-9 from Method 1. Regression lines are given as black solid lines along with associated statistics. Dashed lines represent perfect matches.

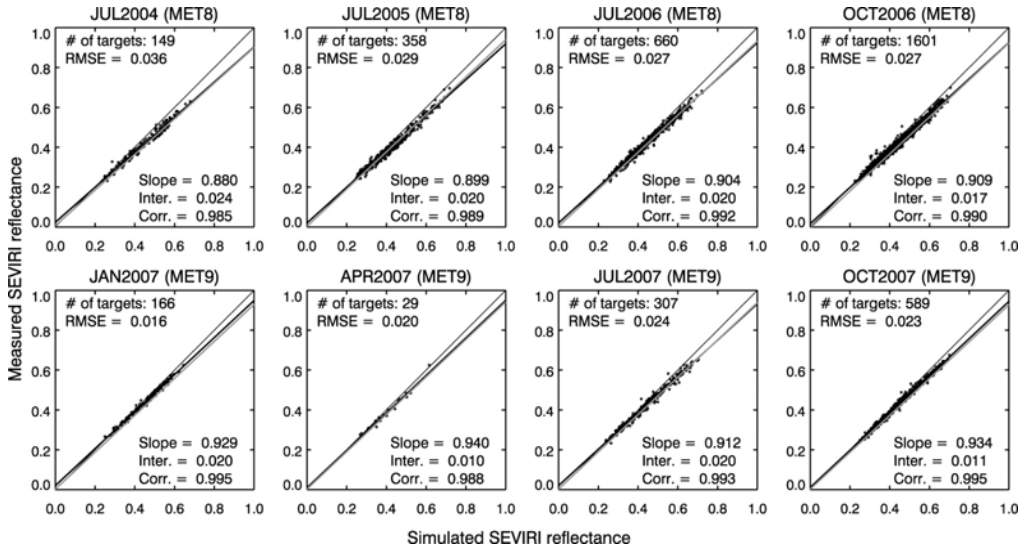

Fig. 8. Scatter plots of simulated vs. measured SEVIRI 0.640-μm channel reflectances of (top) Meteosat-8 and (bottom) Meteosat-9 from Method 2. The simulation is performed for

cloud targets using collocated MODIS cloud products. Linear regression results are displayed as black solid lines along with associated statistics. Regression lines from Method 1 are also displayed as grey solid lines.

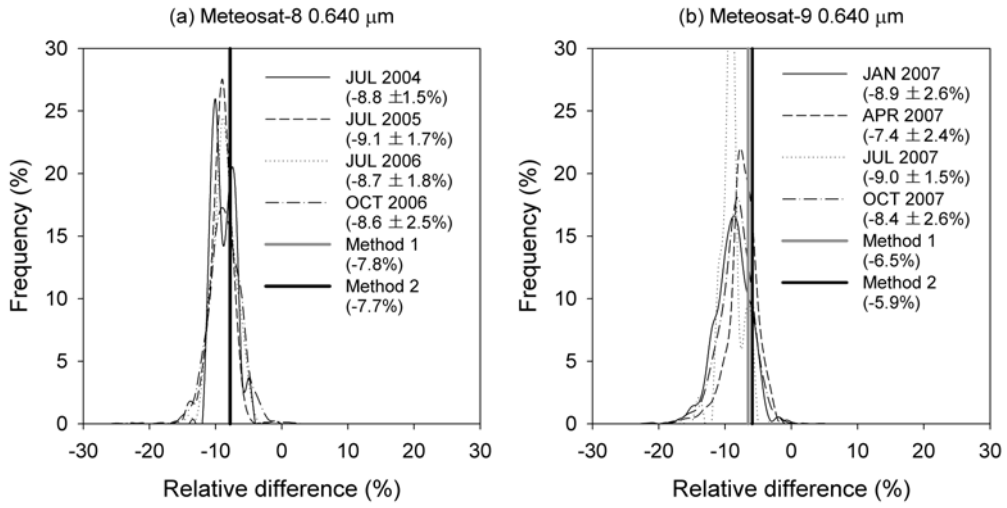

Fig. 9. Monthly frequency histograms of relative differences between measured and simulated reflectances for SEVIRI 0.640-μm channel of (a) Meteosat-8 and (b) Meteosat-9 from Method 3. Mean biases inferred from Methods 1 and 2 are given using grey and black vertical lines, respectively.

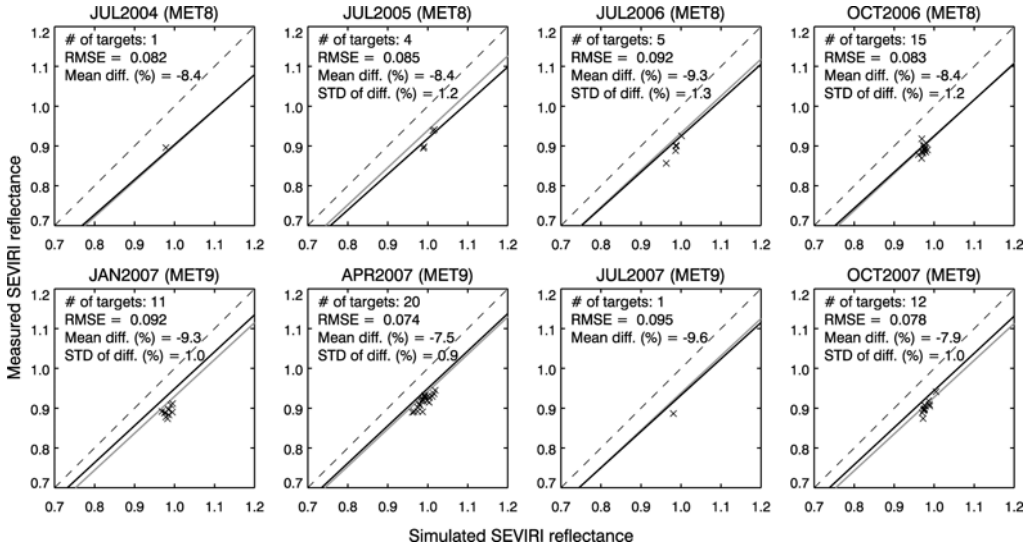

Fig. 10. Comparison of Method 3 (crosses) against Method 1 (grey solid line) and Method 2 (black solid line) for (top) Meteosat-8 and (bottom) Meteosat-9 SEVIRI 0.640-μm channels. For Method 3, the daily average is calculated when the number of selected DCC targets is greater than 10. Dashed lines are perfect matches.

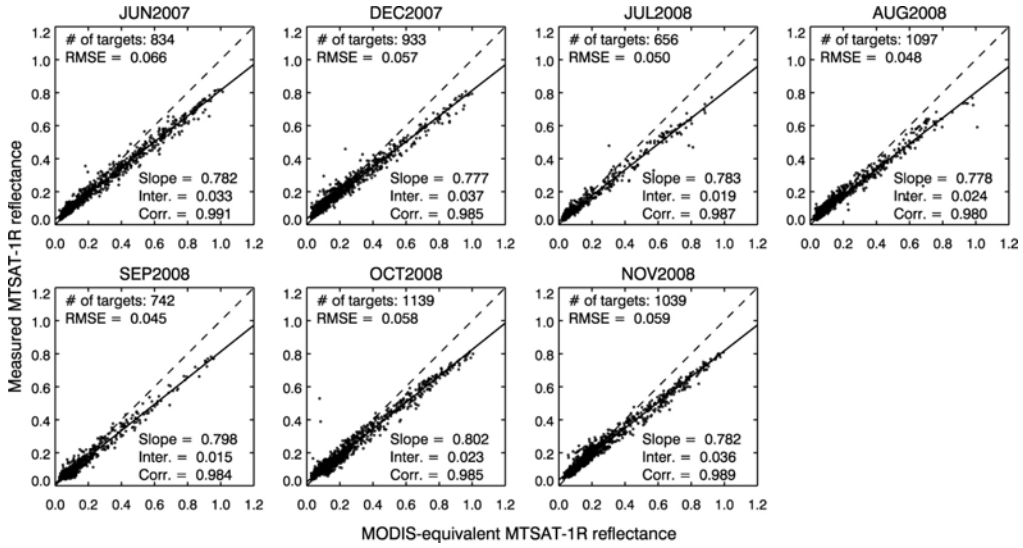

Fig. 11. Same as in Fig. 7 but for the MTSAT-1R 0.724-μm channel (Method 1).

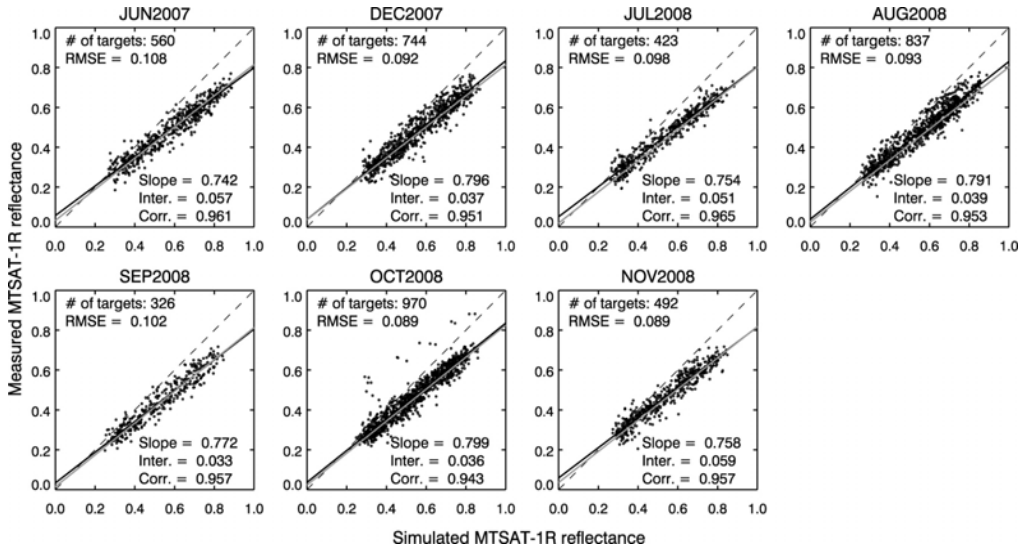

Fig. 12. Same as in Fig. 8 but for the MTSAT-1R 0.724-μm channel (Method 2).

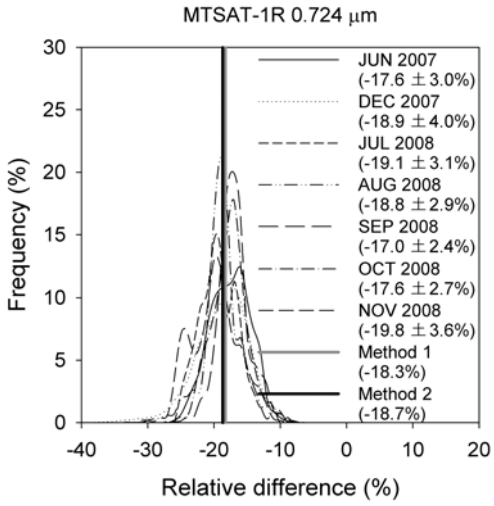

Fig.13. Same as in Fig. 9 but for the MTSAT-1R 0.724-μm channel (Method 3).

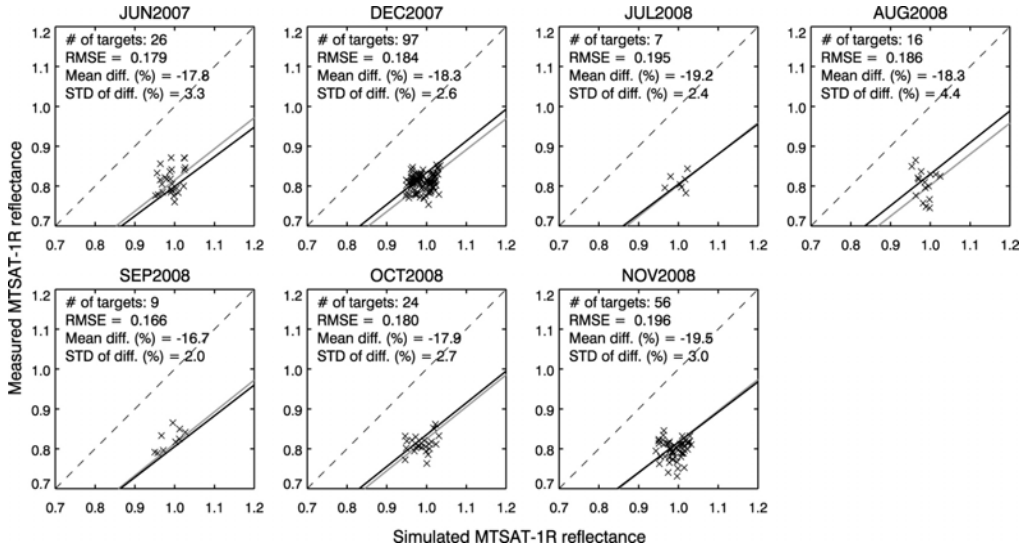

Fig.14. Same as in Fig. 10 but for the MTSAT-1R 0.724-μm channel (Method 3).

21. In general, it would be helpful not only to see scatter plots, correlation coefficients and biases, but also standard deviations. As far as biases are concerned, one should distinguish between relative and absolute biases, and between relative difference and bias (a relative difference for one pixel is not a bias: see for instance Fig. 3 where histograms of relative differences and not histograms of biases are plotted). Furthermore, the authors could consider the use 2D histograms to indicate how the points are distributed along the x = y line: in scatter plots it is not possible to distinguish where the data points are concentrated.

Thanks for the suggestion. In Method 1, MODIS radiance measurements are regarded as a reference, whereas in Methods 2 and 3, simulation results are used as references for

examining SEVIRI and MTSAT-1R visible channel measurements. Therefore, we used the term “bias” for representing the deviation of SEVIRI or MTSAT-1R measurements from the reference values. However, following the reviewer's suggestion, we correct the term “bias” as the “difference between measured and simulated reflectance” in Fig. 3 (now Fig. 9) to avoid confusion. Please note that in the revised version we mainly use regression results instead of mean differences for comparing between Methods 1 and 2. For Method 3, mean values and standard deviation of differences are provided. In order to give consistent index representing the degree of scattering for Methods 1, 2, and 3, we decided to provide root mean square error (RMSE) in each diagram. But 2D histogram may not be necessary because points are hardly overlapped in new monthly plots.

22. Finally, a comparison to the literature like Doelling et al. (2004); Govaerts and Clerici (2004) is missing. In particular, since the presented methods yield different results the consideration of additional calibration sources will be very interesting.

Thank you for pointing out our mistakes. Now obtained results of SEVIRI visible channels are compared with those from Doelling et al. (2004), Jan Fokke Meirink at KNMI (personal communication, 2009), and Govaerts et al. (2004).

[Old]

These results are consistent with the results based on the ray-matching technique between Meteosat-8/9 and MODIS (Jan Fokke Meirink at KNMI, personal communication, 2009), in which Meteosat-8/9 measurements were shown to be biased low 6–7% and the degree of bias of Meteosat-8 was larger than Meteosat-9.

[New]

The calibration results of Meteosat-8/9 visible channels from Method 1 are quite similar to the results from other previous studies based on the ray-matching technique. Doelling et al. (2004) showed that MODIS 0.646-μm channel radiances are shown to be 8% larger than Metoesat-8 0.640-μm channel radiances. In addition, Jan Fokke Meirink at KNMI (personal communication, 2009) compares SEVIRI and MODIS visible channels after the atmospheric correction, showing MODIS 0.646-μm channel reflectances 7% (6%) larger than Meteosat-8 (Meteosat-9) 0.640-μm channel reflectances. All these results commonly assert low measurement biases of SEVIRI 0.640-μm channels, implying that the operational calibration of Meteosat visible channels using ocean and desert targets (Govaerts et al., 2004) may underestimate the visible channel reflectance.

23. In this context, is the observed difference in calibration accuracy obtained from Method 1 and Method 3 for SEVIRI really related to a saturation effect? How is the design

specification of the channel range? Does the 10 bit SEVIRI digitalisation of the signal play any role?

Dynamic range of SEVIRI 0.640-μm channel is 0–533 W m^{-2} sr^{-1} μm^{-1}, corresponding to 0–1.04 of reflectance for SZA = 0°. Since DCC targets have high reflectances around 1, higher biases in Method 3 are interpreted as saturation of SEVIRI visible channels. Note that such deviation is not shown in the MTSAT-1R visible channel in spite of much larger scatterings. However, we are not able to provide definite answers because raw data before the pixel level are not considered in this study. This topic may be beyond the current research scope and thus should deserve a separate examination.

Further comments:

24. Abstract: Please mention the time periods investigated for the two satellite instruments.

Time periods for the investigation are now included.

[Old]

To examine the calibration performance of the Meteosat-8/9 Spinning Enhanced Visible Infra-Red Imager (SEVIRI) 0.640-μm and the Multi-functional Transport Satellite (MTSAT)-1R 0.724-μm channels, three calibration methods were employed.

[New]

To examine the calibration performance of the Meteosat-8/9 Spinning Enhanced Visible Infra-Red Imager (SEVIRI) 0.640-μm and the Multi-functional Transport Satellite (MTSAT)-1R 0.724-μm channels, three calibration methods were employed. Total eight months during the 2004–2007 period are used for SEVIRI, and total seven months during the 2007–2008 period are used for MTSAT-1R.

25. Abstract, page 12630, line 11–13: "In the simulation, the three-dimensional radiative effect of clouds was taken into account and was subtracted from the simulated reflectance to remove the simulation bias caused by the plane-parallel assumption.": In principle, the authors do not do a full 3D radiative transfer simulation and they do not know the magnitude of these 3D effects in detail, but they try to minimise them. Please reformulate this sentence.

Following the comment, we modify the sentence as follows:

[Old]

In the simulation, the three-dimensional radiative effect of clouds was taken into account and was subtracted from the simulated reflectance to remove the simulation bias caused by the plane-parallel assumption.

[New]

In the simulation, cloud three-dimensional (3D) radiative effect associated with subgrid variations is taken into account using the lognormal-independent column approximation (LN-ICA) to minimize the simulation bias caused by the plane-parallel assumption.

26. Abstract, page 12630, line 18–21: Method 2 and Method 3 provide very similar results (see above), while Method 3 yields differences that are not fully understood. Thus, I would say that the three methods can yield valuable information to monitor the calibration performance, but I am not sure whether a combination of them is really necessary.

For case of MTSAT-1R visible channels, three methods show fairly good agreements in the calibration results. We believe that the independent Method 3 should provide results in line with Methods 1 and 2 if calibration is done properly. From this point of view, we suspect saturation of SEVIRI visible channels in the high end of reflectance. Therefore, we think that the combination of three methods provides a more efficient way to monitor calibration performance of targeted visible channels.

27. Page 12632, line 7: Please explain why the target for the maximum calibration uncertainty is 5 %.

For the reliable retrieval of meteorological parameters from the satellite observations, a certain level of accuracy of radiometric calibration is required. Especially, long-term monitoring requires more strict calibration accuracy (~2%) than short-term monitoring (~5%). However, many operational calibration systems, particularly not equipped with onboard calibrator, aim at a 5% calibration accuracy for practical reasons. It is already a challenge to meet the 5% uncertainty level. For example, SEVIRI calibrations aim at an order of 5% accuracy for the analysis of meteorological variables (Schmetz et al., 2002), and it has been argued that those accuracy requirements can be achieved from vicarious calibration methods using ocean and desert targets (Govaerts and Clerici, 2004). We add some references to generalize this discussion in the text.

[Old]

However, because of the relatively small reflectance values (<0.5) of these targets, small errors in input data may result in significant relative errors in simulated values, exceeding the targeted 5% relative uncertainty.

[New]

However, because of the relatively small reflectance values (<0.5) of these targets, small errors in input data may result in significant relative errors in simulated values, exceeding

targeted 5% of the relative uncertainty (e.g., Arriaga and Schmetz, 1999; Knapp and Vonder Haar, 2000; Govaerts et al., 2001, 2004; Govaerts and Clerici, 2004).

Arriaga, A. and Schmetz, J.: Calibration of the Meteosat-5/-6 VIS Channels with Help of Modelled Radiances, Contrib. Atmos. Physics, **72,** 133–139, 1999.

Govaerts, Y., Arriaga, A., and Schmetz, J.: Operational vicarious calibration of the MSG/SEVIRI solar channels, Adv. Space. Res., 28, 21–30, doi:doi:10.1016/S0273-1177(01)00269-1, 2001.

Govaerts, Y. and Clerici, M.: MSG-1/SEVIRI Solar Channels Calibration Commissioning Activity Report, EUMETSAT Technical Note EUM/MSG/TEN/04/0024, EUMETSAT, 2004.

Govaerts, Y. M., Clerici, M., and Clerbaux, N.: Operational calibration of the Meteosat radiometer VIS band, IEEE T. Geosci. Remote Sens., 42, 1900–1914, 2004.

Knapp, K. R. and Vonder Haar, T. H.: Calibration of the eighth Geostationary Observation Environmental Satellite (GOES-8) imager visible sensor, J. Atmos. Oceanic Tech., 17, 1639–1644, 2000.

Schmetz, J., Pili, P., Tjemkes, S., Just, D., Kerkmann, J., Rota, S., and Ratier, A.: Radiometric performance of SEVIRI, Bull. Amer. Meteor. Soc., 977–992, 2002.

28. Page 12632, line 13: Please cite older authors like Vermote and Kaufman (1995); Govaerts et al. (2001); Hu et al. (2004).

Now cited.

29. Page 12634, line 13: "to reduce navigation errors." –> "to reduce navigation errors and parallax effects."

Corrected.

30. Page 12636, line 21: How do the authors come to this value of 227 K?

It is included in #6.

31. Page 12636, line 27: "optical properties of mixed-phase" –> "optical properties of potentially mixed-phase": one could have supercooled water droplets.

Now corrected.

32. Page 12639, line 4–5: Please make a complete list of all the conditions used: SZA≤ 40° (why "e.g., ≤ 40°"?), which homogeneity checks and so on?

Now all thresholds are explained when discussing PPH biases. Changed parts are included in #19.

33. Page 12639, line 20–24: Why does the bias depend on the magnitude of the reflectance?

When the correct space count offset is not provided in operational calibration, bias of calibrated reflectance can change with reflectance magnitude. This is evidently shown for MTSAT-1R channel because regression intercept is considerably large (>0.02) and regression slope is around 0.8. As a result, it is inferred that measurement bias is positive in case of reflectance < 0.2, and the bias turns into negative for larger reflectances. For SEVIRI visible channels, regression offsets are relatively small, and thus dependence of the degree of measurement bias to the reflectance magnitude is much weaker compared to MTSAT-1R visible channel, showing similar degree measurement biases within 6–7% except the high end side of reflectance.

34. Page 12643, line 7: Please quantify the scatter mentioned here.

We employ RMSE to represent the degree of scattering in the diagram.

[Old]

The larger scatter observed by each comparison is not likely derived from gaseous absorption, such as water vapor absorption around 0.724 μm, as the DCC targets used in Method 3 were not sensitive to water vapor but exhibited the same degree of scatter.

[New]

Furthermore, it is suggested that the large scattered patterns found in MTSAT-1R results from Methods 1 and 2 (two or three times larger than RMSEs of Meteosat-8/9) are not likely due to the water vapor absorption around 0.724 μm. It is because the DCC results showing the same degree of scattering should not be sensitive to the water vapor absorption, as seen in the comparison between Fig. 10 and Fig. 14.

35. Page 12654, Table 1: Please explain the meaning of "varying from 0.1 to 1.0 with a 0.1 increment". If you binned the MODIS data, does 0.1 mean that you took MODIS reflectances between 0.0 and 0.1 (0.0 ≤ refl < 0.1)? In that case, the mean values of the MODIS reflectances in the given intervals should be given as well.

Because deviation of measured reflectance from reference value is estimated using regression equation in Method 1, we do not need binned MODIS data. The deviation is calculated exactly for 0.1, 0.2, 0.3, …., 0.9, and 1.0. Please note that Table 1 is no longer valid in the revised version because the table is superfluous in comparing three calibration methods.

36. Page 12655, Table A1: How does the ICA perform?

The way to obtain ICA reflectance in Table A1 is described in more detail, i.e.:

[Old]

This is based on the fact that MODIS visible channel reflectances can be accurately calculated with less than 3% uncertainty using cloud parameters of MODIS products on a pixel basis (Ham et al. 2009). However, if we consider a large grid size and assume a homogenous cloud layer at each grid using averaged cloud parameters for the radiative transfer calculation, the PPH bias would be generated in the simulations. Because the modeling accuracy is known on the pixel basis, the differences between simulated and observed MODIS reflectances for the larger area can be interpreted as the PPH biases; that is:

$$\Delta R_{PPH} \cong R_{sim}(\langle\tau\rangle) - \langle R_{obs}(\tau)\rangle \qquad \text{(A2)}$$

where subscripts “sim” and “obs” denote simulated and observed reflectances, respectively.

[New]

The estimation of PPH biases is firstly based on the fact that MODIS visible channel reflectances at a pixel point can be accurately calculated with less than 3% uncertainty using cloud parameters of MODIS products (Ham et al. 2009). This suggests that grid-mean values of simulated and measured reflectances are expected to be nearly same. Therefore, we replace the second term in Eq. (7) with measured grid reflectances to represent ICA reflectance, i.e.:

$$\Delta R_{PPH} \cong R_{sim}\left(\frac{1}{N}\sum_{i=1}^{N}\tau_i\right) - \frac{1}{N}\sum_{i=1}^{N}R_{obs}(\tau_i) \cong R_{sim}(\langle\tau\rangle) - \langle R_{obs}(\tau)\rangle \qquad (8)$$

where subscripts “sim” and “obs” denote simulated and observed reflectances, respectively. This is an efficient way to calculate ICA reflectances because only average of measured pixel reflectances in a grid box is needed. On the contrary, for obtaining ICA reflectance from the radiative simulation, all sub-pixel reflectances in one grid box are needed. For example, cloud reflectances at about 2500 sub-pixel points should be known for the estimation of ICA reflectance at a 0.5°-grid box from MODIS-measured cloud fields. Realistic approach may be impossible because of the computational burden, and thus we later adopt an approximate method to compute ICA reflectances for SEVIRI and MTSAT-1R channel calibrations.

37. Page 12659, Fig. 3: "Monthly frequency histograms of measurement biases from simulated values at SEVIRI 0.640-μm channels of (a) Meteosat-8 and (b) Meteosat-9 form Method 3. Relative errors are given for the measured reflectances as percentage errors from simulated values. Mean biases inferred from the ray-matching method (Method 1) are also given as vertical grey solid lines." –> "Monthly frequency histograms of relative differences between measured and simulated reflectances for SEVIRI 0.640-μm channel of (a) Meteosat-8 and (b) Meteosat-9 from Method 3. Mean biases inferred from the ray-matching method (Method 1) are also given as vertical grey solid lines."

Now corrected.

38. Page 12660, Fig. 4: The x axis range selected makes it clear that high reflectances are observed here. However, a smaller scale (e.g. 0.8–1.1 in the x axis) could enable to observe some more detail of the data cloud. Please consider whether it could be more useful to zoom into the graph and change the scales.

Taking the suggestions, axis range is changed from 0–1.0 into 0.7–1.2. Modified figures are included in #20.

39. Page 12662, Fig. A1: It is not really clear from this figure whether the biases become smaller when the grid spacing is increased. In particular, for the 0.3° grid size, it seems that new larger biases appear that were not present in the 0.2° grid size plot. Why is it like this?

This figure represents the magnitude of PPH biases. It is shown that PPH bias increases with subgrid variability and grid size. Therefore, we recommend a smaller grid size representing a smaller subgrid variability for minimizing PPH biases. Because the conversion into 0.5°-grid data is indispensable for collocating between two satellites in Method 2, we apply a threshold condition of $STD(R_{0.646}) \leq 0.1$ to select homogenous cloud targets. However, even if the homogeneity check is applied to select targets, positive PPH biases are still expected, as marked as a grey box in Fig. A1 (now Fig. 4), implying that subgrid variability should be counted for accurate simulations. That is why we employ the LN-ICA method to calculate SEVIRI and MTSAT-1R visible channel reflectances. This discussion is now included in section 2.2 when examining 3D effects.

40. Page 12664, Fig. A3: Is the ICA bias here an absolute or relative bias?

It is absolute bias. When defining the simulation bias associated with 3D effects, we use an absolute manner by following terms in other previous studies (e.g., Cahalan et al., 1994a, b).

Technical corrections

Thanks for careful reading. Now all terms are changed following your suggestion.

• Please replace the use of the past tense in expressions like "In this study, we explored..." with the use of the present "In this study, we explore..." throughout the whole paper.
• Please check the usage of "grid" and correct it when needed: in many cases ("at each grid...") a grid box is meant and not the grid itself.
• Page 12631, line 4: "may be changed" –> "may change".
• Page 12631, line 12: "The inter-satellite calibration method" –> "Inter-satellite calibration".
• Page 12631, line 23: "the vicarious calibration" –> "vicarious calibration".
• Page 12631, line 27: "surface properties, desert" –> "surface properties, deserts".
• Page 12631, line 28: Please cite one of the older papers like Fraser and Kaufman (1986).
• Page 12631, line 28: "Knapp and Haar" –> "Knapp and Vonder Haar".
• Page 12633, line 1: "solar channel" –> "solar channels".
• Page 12634, line 20: "(SZA)" –> "SZA".
• Page 12635, line 5: "MTSAT" –> "MTSAT-1R".
• Page 12636, line 6: "As in the Method 1" –> "As in Method 1".
• Page 12636, line 7: "data remained" –> "data was considered".
• Page 12636, line 12: "of less than" –> "smaller than".
• Page 12637, line 18–20: "The SBDART model considers the multiple scatterings by atmospheric particles under the assumption of the plane-parallel atmosphere." –> "The SBDART model considers multiple scattering by atmospheric particles under the assumption of a plane-parallel atmosphere.".
• Page 12638, line 5: "two homogeneous conditions" –> "two homogeneity conditions".
• Page 12638, line 10: "to monitor" –> "to ensure".
• Page 12639, line 14: "were selected" –> "was selected".
• Page 12640, line 20: "smaller those" –> "smaller than those".
• Page 12640, line 27: Please remove "The biases were given in a percentage ratio.".
• Page 12641, line 5: "in the Method 3" –> "in Method 3".
• Page 12641, line 13: "However, explanation" –> "However, a more detailed explanation".
• Page 12642, line 1: What is JAMI?
JAMI is the name of sensor aboard MTSAT-1R. It is defined when describing used dataset.

• *Page 12642, line 15: "may due to the scan problems" –> "may be due to scan problems".*

• *Page 12642, line 26: What does "monthly modes" mean?*

Please note that in the revised version, monthly mean and associated standard deviation are used instead of the mode to represent results of Method 3.

• *Page 12642, line 29: "from SEVIRI visible" –> "for the SEVIRI visible".*

• *Page 12643, line 17: "covert" –> "convert".*

• *Page 12644, line 5: "small SZAs" –> "moderate SZAs".*

References

Doelling, D., Nguyen, L., and Minnis, P.: Calibration comparisons between SEVIRI, MODIS, and GOES data, in: EUMETSAT Meteorological Satellite Conference, Prague, Czech Republic, pp. 77–83, 2004.

Fraser, R. S. and Kaufman, Y. J.: Calibration of satellite sensors after launch, Appl. Opt., 25,1177–1185, 1986.

Govaerts, Y. and Clerici, M.: MSG-1/SEVIRI Solar Channels Calibration Commissioning Activity Report, EUMETSAT Technical Note EUM/MSG/TEN/04/0024, EUMETSAT, 2004.

Govaerts, Y., Arriaga, A., and Schmetz, J.: Operational vicarious calibration of the MSG/SEVIRI solar channels, Adv. Space. Res., 28, 21–30, doi:doi:10.1016/S0273-1177(01)00269-1, 2001.

Ham, S.-H., Sohn, B.-J., Yang, P., and Baum, B. A.: Assessment of the Quality of MODIS Cloud Products from Radiance Simulations, Journal of the Applied Meteorology and Climatology, 48, 1591–1612, doi:10.1175/2009JAMC2121.1, 2009.

Hu, Y., Wielicki, B., Yang, P., Stackhouse, P.W., J., Lin, B., and Young, D.: Application of deep convective cloud albedo observation to satellite-based study of the terrestrial atmosphere: monitoring the stability of spaceborne measurements and assessing absorption anomaly, Geoscience and Remote Sensing, IEEE Transactions on, 42, 2594 – 2599, doi:10.1109/TGRS.2004.834765, 2004.

Oreopoulos, L. and Davies, R.: Plane parallel albedo biases from satellite observations. PartII: Parameterization for bias removal, Journal of Climate, 11, 933–944, 1998.

Sohn, B.-J., Ham, S.-H., and Yang, P.: Possibility of the Visible-Channel Calibration Using Deep Convective Clouds Overshooting the TTL, Journal of the Applied Meteorology and Climatology, 48, 2271–2283, doi:10.1175/2009JAMC2197.1, 2009.

Vermote, E. and Kaufman, Y.: Absolute calibration of AVHRR visible and near infrared channels using ocean and cloud views, Int. J. Remote Sensing, 95, 2317–2340, 1995.

Zinner, T., Mayer, B., and Schröder, M.: Determination of 3D cloud structures from high resolution radiance data, Journal of Geophysical Research, 111,

doi:10.1029/2005JD006 062, 2006."